Title
Experimental Investigation of Pressure-Controlled Boiling for Rapid Transient Cooling

Author
Ma, Matthew Xiaoyu

Publication Date
2021

Peer reviewed|Thesis/dissertation

UNIVERSITY OF CALIFORNIA

Los Angeles

Experimental Investigation of Pressure-Controlled Boiling for Rapid Transient Cooling

A thesis submitted in partial satisfaction
of the requirements for the degree Master of Science
in Mechanical Engineering

by

Matthew Xiaoyu Ma

2021

ABSTRACT OF THE THESIS

Experimental Investigation of Pressure-Controlled Boiling for Rapid Transient Cooling

by

Matthew Xiaoyu Ma

Master of Science in Mechanical Engineering

University of California, Los Angeles, 2021

Professor Timothy S. Fisher, Chair

Flash boiling is a two-phase cooling method based on the phenomenon of flash boiling in which a working fluid is rapidly vaporized upon sudden depressurization, allowing for rapid cooling through conversion of the fluid's sensible heat to latent heat. In this process, the sensible heat of surrounding environment around the working fluid decreases. Therefore, flash cooling is a promising candidate for transient thermal management. The phase-change process associated with flash boiling differs from traditional thermally-driven boiling, as flash boiling inception is controlled by a different thermodynamic variable – pressure. Consequently, by allowing pressure to be the driving factor, temperature becomes a variable performance metric for flash cooling in practical devices. To better understand the nature of flash boiling incipience and measure flash cooling rates, experiments were constructed to measure depressurization wave propagation through a tube and transient flash cooling in a vapor chamber for various configurations and heating loads. Additionally, a metric for flash cooling based on time constants is presented to help quantify transient cooling performance.

The thesis of Matthew Xiaoyu Ma is approved.

Hossein Pirouz Kavehpour

Adrienne S. Lavine

Timothy S. Fisher, Committee Chair

University of California, Los Angeles

2021

TABLE OF CONTENTS

LIST OF FIGURES

LIST OF TABLES

LIST OF SYMBOLS

A	Surface area, (m^2)
α	Flash cooling curve-fitting parameter, (W)
β	Flash cooling curve-fitting parameter, (s)
C_2	Parameter derived from contact angle
$C_{p,copper}$	Heat capacity of copper, (J/kg $\cdot$ K)
D_c	Nucleating cavity mouth diameter, (m)
$\dot{E}_{in}$	Energy input rate, (W)
E_{max}	Theoretical maximum total cooling energy over certain time interval, (J)
$\dot{E}_{out}$	Energy output rate, (W)
E_p	Total cooling energy over certain time interval, (J)
$\dot{E}_{st}$	Energy storage rate, (W)
ϵ	Emissivity
η	Cumulative flash efficiency
h	Enthalpy, (J/kg)
h_{ext}	Heat transfer coefficient between vapor chamber and ambient environment, ($W/m^2 \cdot K$)
h	Planck's constant, ($J \cdot s$)
h_{fg}	Heat of vaporization, (kJ/kg)
h_f	Enthalpy of fluid before flashing, (kJ/kg)
h_g	Enthalpy of fluid after flashing, (kJ/kg)
J	Rate at which activated clusters appear per unit volume of liquid per unit time, ($1/(cm^3 \cdot s)$)
k_b	Boltzmann's constant, (J/K)
k_l	Thermal conductivity of liquid, ($W/(m \cdot K)$)
m	Lumped mass, (kg)
$m_{methanol}$	Mass of methanol, (kg)
$m_{vapor\ chamber}$	Mass of vapor chamber, (kg)

N	Number of molecules per unit volume, $(1/m^3)$
P	Input power of heater, (W)
P	Pressure, (Pa)
P_b	Bubble saturation pressure, (Pa)
P_{sys}	System pressure, (Pa)
q	Applied wall heat flux, (W/m^2)
q_{fc}	Cooling rate due to flash, (W)
$q_{fc,max}$	Maximum experimental flash cooling (W)
$q_{fc,fitted}$	Curve-fit flash cooling rate, (W)
$q_{max,p}$	Theoretical maximum flash cooling, (W)
q_{nc}	Cooling rate due to natural convection, (W)
q_{rad}	Cooling rate due to radiation, (W)
ρ_v	Vapor density, (kg/m^3)
σ	Stefan-Boltzmann constant, $(W/(m^2 \cdot K^4))$
σ	Surface tension, (N/m)
t	Time, (s)
τ_1	First curve-fitting time constant, (s)
τ_2	Second curve-fitting time constant, (s)
$T(t)$	Temperature, (K)
T_a	Ambient room temperature, (K)
T_{crit}	Incipient liquid superheat temperature, (K)
$T_{w/o\ flash}(t)$	Thermal response of vapor chamber under step heating with no flash, (K)
T_l	Liquid temperature, (K)
$T_{w/\ flash}(t)$	Thermal response of vapor chamber under step heating with flash, (K)
T_{sat}	Saturation temperature corresponding to system pressure, (K)
θ	Contact angle, (°)

ACKNOWLEDGEMENTS

I'd like to express my greatest thanks to my advisor, Prof. Fisher for providing me the opportunity to carry out this research project, giving me much guidance and support, and allowing me to expand upon my skillsets professionally, interpersonally, introspectively, and more. Thanks to the support of the Center for Integrated Thermal Management of Aerospace Vehicles for opportunities for me to discuss and connect my research with industry partners. Mentorship from Dr. Barako and Dr. Bar-Cohen have also been invaluable and precious. Also, experiments wouldn't have been possible without the generosity of Dr. North in providing vapor chamber samples for testing. Thanks to fellow lab members Ujash Shah, Yuan Hu, Indronil Ghosh, and Kaiyuan Jin for answering my questions, offering their specialized hand, and helping me in many ways, many times. Chapter Four is a version of [1.3.17] and greatly benefited from collective thoughtful discourse.

No destination is met without a having a journey along the way, and so I'd like to also give thanks to the many professors whose classes have satisfied and expanded my knowledge, and allowed me to build new connections and friends along the way. UCLA is a wonderful institution and it has been an honor to have been part of the greater pursuit of knowledge. Thanks for all the memories.

Lastly, thanks to those that have given me more than they have received, and thanks to you, the curious reader.

Chapter 1: Introduction

1.1 Motivation

As electronic power consumption continues to increase due to semiconductor scaling, the need for adequate cooling becomes more and more important as the threat of thermal runaway becomes increasingly of concern. Thermal management for next-generation devices should address not only the high-heat fluxes associated with such devices, but also the transient operation as large changes in power are applied over short times. Temperature is often used as an engineering metric to assess the performance and operability of devices under heating loads, and so, optimal device functionality requires stringent temporal control for both transient and steady-state operation.

Optimal design for transient thermal management should include dynamic cooling, as traditional thermal design focuses on steady-state operation that is inadequate for the short time scales associated with transient phenomena. A couple of noteworthy examples of applications where devices operate for a short duration include both pulsed laser operation [1.1.1] in which case temperature stability is crucial for maintaining consistent spectral distribution, and radar systems for aiding aircraft landing in degraded visual environments [1.1.2].

In this work, an experimental framework was built to elucidate important factors associated with transient cooling based on the phenomenon of flash boiling. As with any multi-phase convective cooling solution, phase-change associated with flash boiling is an efficient means of heat removal, as modest amounts of working fluid can achieve appreciable cooling rates due to the high latent heat of vaporization of the liquid working fluid. Topics of discussion in this work include: insight into flash incipience, application of flash cooling for a vapor chamber configuration under steady-state and dynamic heat loads, analysis of the transient cooling

performance, and insight into metrics that can be used to quantify flash cooling efficacy. The working principles behind flash boiling are discussed in the following section.

1.2 Background

A pressure-temperature (P-T) diagram is useful in explicating the thermodynamic requirements for phase-change and its relevance to flash boiling. Fig. 1.2.1 shows the P-T diagram for methanol, the working fluid of choice for our studies. Please refer to the Appendix A.1 for more information on the choice of working fluid. The working fluid, initially at ambient conditions denoted by the blue point in Fig. 1.2.1, exists as a subcooled liquid. In order to vaporize, the liquid must first cross the saturation curve into the vapor domain. This process can be achieved in two typical ways: (1) increase temperature at constant pressure, as denoted by the purple line, or (2) decrease pressure at constant temperature, as shown by the vertical red line.

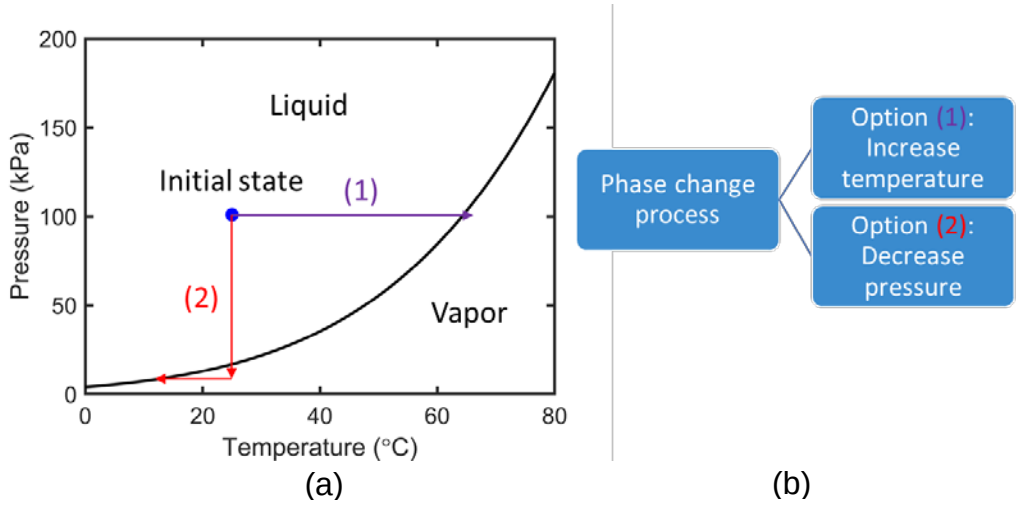

Fig. 1.2.1: Thermodynamics of flash boiling. (a) P-T diagram for methanol. (b) Mechanisms for phase-change.

The aforementioned first method requires sufficient heat input to overcome the thermal mass of the system that contains the working fluid. Compared to the first method, the latter can be quickly realized through rapid depressurization, and is known as a flashing process. With rapid depressurization, the liquid transitions from a subcooled liquid to a metastable superheated

liquid, and begins to boil upon perturbation. (Conventionally, liquid superheat is defined as the difference between the liquid temperature and the saturation temperature of the liquid at the system pressure.) During the boiling process, the fluid cools, as energy for phase-change is supplied by the bulk liquid, until the saturation temperature for the reduced pressure is met, as shown by the horizontal red line in Fig 1.2.1. As a pressure-driven process, flash boiling is applicable where phase-change is desirable, as discussed in the next section.

1.3 Historical timeline of flash boiling

A couple of notable examples of flash boiling are briefly summarized to demonstrate the applicability of flash boiling in industry. These applications use the vapor, extracted directly from the liquid, to drive processes for energy generation and liquid purification. Such applications include flash steam geothermal power generation and flash desalination. Flash steam geothermal power plants, the most common utilization of geothermal energy, convert thermal energy from within Earth's core to electrical energy by using vapor to drive steam turbines [1.3.1]. Water deep within the Earth exists as a high-pressure, high-temperature liquid, and is pumped up to a flashing drum at the surface, where the lower-pressure environment enables the liquid to flash into steam. The steam then passes through a turbine, which produces electricity. Steam exiting the turbine is then condensed and reinjected into the ground, where it is subsequently reheated by Earth's natural internal thermal energy. This cycle then repeats, acting as a renewable and sustainable energy source. Another application of flash boiling is flash desalination, in which a thermal process is used to convert seawater into distilled water [1.3.2]. Seawater is preheated and exposed to low pressure to induce flashing. The flashed vapor is then condensed and extracted as distilled water. However, since the liquid requires pre-heating before flashing, this technique for desalination is more energy intensive than non-thermal ones, namely reverse osmosis.

Aside from applications in which flash boiling is necessary for some process, one instance in which flash boiling is undesirable is in the nuclear industry. Pressurized water reactors, the

most common utilization of nuclear power in the US [1.3.3], use energy from nuclear fission to heat pressurized water flowing within the reactor core. This heated water, as a superheated liquid, then flows through a heat exchanger in which water flowing through a secondary system vaporizes to produce steam, which subsequently flows through a turbine to generate electricity. For relevance to flash boiling, it is the loss of structural integrity of the fluid system handling the superheated water that is of concern. In such cases, loss of coolant accidents (LOCA) due to piping rupture allows for sudden depressurization of the superheated water, leading to explosive vaporization. From a historical perspective, LOCA-induced destruction was partly responsible for damage to the nuclear reactor core that led to the Chernobyl disaster [1.3.4].

The aforementioned examples illustrate the use of flash boiling in which vaporization plays crucial roles, but with minimal relation to the cooling phenomena as a result of the phase-change phenomenon. Here, some examples of flash cooling in industrial applications are presented. Flash cooling has found success in the aerospace industry, where the space environment provides the ideal vacuum reservoir without the need for additional hardware to achieve equivalent depressurization. Specifically, flash evaporator systems were used on the space shuttles as primary cooling during ascent and reentry. In those systems, water, the working fluid of choice, was sprayed onto Freon cooling loops in either high load or topping evaporators, supporting up to 43 kW of cooling [1.3.5]. The byproduct of the flash process, steam, is vented overboard and can additionally act as a propulsive source. There also exists commercial implementation of flash cooling systems. The V-chiller is designed for cooling beverages at a rate of 4 cans per minute, providing on-demand cooling [1.3.6]. By allowing for rapid cooling, the need for continuous cooling is eliminated, allowing V-chiller to operate at a substantially lower energy consumption compared to typical vapor-compression refrigeration systems. Another example of a flash cooling system is a patented rapid cooling apparatus for food processing [1.3.7], in which hot liquid (for later consumption) to be cooled flows through coils immersed in working fluid that

undergoes flashing [1.3.8]. The container housing the working fluid is connected to a vacuum pump, and exposure to low pressures allows the working fluid to extract heat from the hot liquid as it boils.

In terms of academic work, there have been previous insights into thermophysical factors that affect flash, and the nature of flash boiling. Sudden depressurization of a pressurized liquid container leads to LOCA in which the coolant flashes, and this phenomenon has been studied in the nuclear reactor industry in which effects of LOCA must be mitigated [1.3.9]. These studies capture the pressure variations in time, but little work has been found to analyze the heat transfer during such a process. Sudden depressurization and subsequent rapid boiling have been studied in other prior work. Hanaoka et al. experimentally demonstrated low inception superheats for flash evaporation similar to homogeneous boiling [1.3.10]. Zhang et al. confirmed the importance of initial fluid conditions in determining transient liquid temperature, which is an important consideration for transient convective flash cooling [1.3.11]. Saury et al. present an experimental study of the effect of liquid amounts and depressurization on flash [1.3.12].

Other studies on flash boiling include the rate of depressurization and other geometric factors, as investigated by Hahne et. al [1.3.13]. Since depressurization-associated dynamics is the driving proponent of flash boiling, the nature of the depressurization wave propagation through a two-phase mixture is considered by Miyazaki et al. [1.3.14]. More recently, flash evaporation has been analyzed for spray cooling [1.3.15], and models have been developed to understand isolated bubble dynamics during flash [1.3.16], but little progress has occurred on a transient model or correlation for heat removal during flash. The bulk of the experimental work presented in chapter 4 of this thesis addresses some of the shortcomings associated with quantification of transient, step heat removal during flash and also presents metrics to gauge its efficacy. This work was done using a vapor chamber setup and is coauthored in an upcoming publication [1.3.17].

Chapter 2: Factors that affect flash incipience

2.1 Motivation

To investigate the nature of flash cooling, we first reviewed conventional, temperature controlled boiling theory and adapted it in a way in which the dependent variable is no longer a temperature difference, but a pressure difference. This shift in perspective allows for insight into how active control of the system pressure affects conditions within the liquid working fluid to promote bubble nucleation. First, the criterion for superheat is established, for both homogeneous and heterogeneous nucleation.

2.2 Depressurization induced boiling

In flash boiling, bubbles form within the bulk of the fluid, away from walls and surfaces, similar to that observed during homogeneous nucleation. As such, we looked to quantify the superheat for homogeneous boiling, from a pressure-controlled perspective. For homogeneous nucleation, it is assumed that nucleation occurs when excess availability of clusters of activated molecules reaches a maximum. From kinetic theory, assuming the rate at which activated clusters form is proportional to the frequency of molecular collisions and that the pressure in the cluster of activated molecules can be related to the mechanical equilibrium condition, the governing equation for homogeneous nucleation [2.2.1] is expressed as:

$$\Delta P \equiv P_b - P_{sys} = \frac{2\sigma}{\left[\frac{3k_b T_{crit}}{4\pi\sigma}\ln\left(\frac{Nk_b T_{crit}}{Jh}\right)\right]^{\frac{1}{2}}} \tag{1}$$

where P_b is bubble saturation pressure (Pa) and corresponds to T_{crit}, P_{sys} is system pressure (Pa), σ is surface tension of liquid (N/m), k_b is Boltzmann's constant (J/K), T_{crit} is the incipient liquid superheat temperature (K), N is number of molecules per unit volume ($1/\mathrm{m}^3$), J is an assumed rate at which activated clusters appear per unit volume of liquid per unit time ($1/(\mathrm{cm}^3 \cdot \mathrm{s})$), and h is Planck's constant ($\mathrm{J} \cdot \mathrm{s}$). Eqn. (1) is plotted for various assumed values of J.

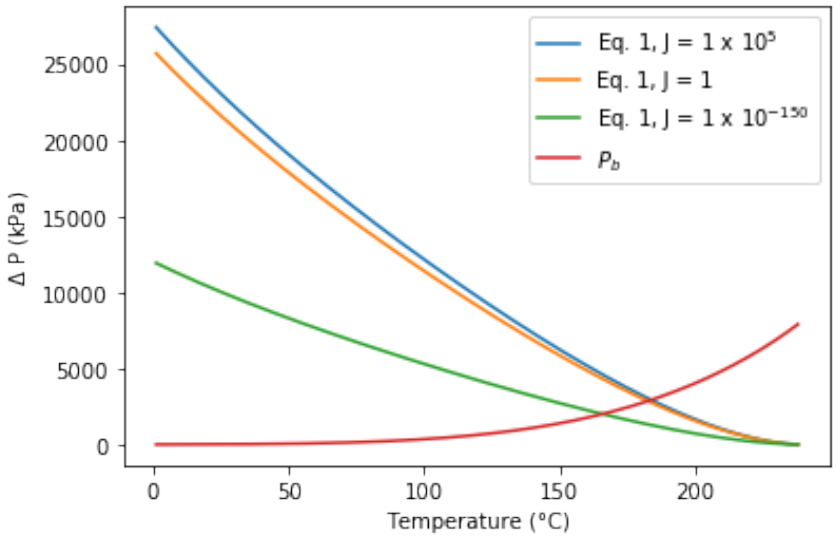

Fig. 2.2.1: Change in pressure required for homogeneous nucleation, for various values of J.

The intersection of the curve labeled P_b and that corresponding to a particular value of J gives the maximum temperature that the liquid can sustain before the onset of phase-change for a full vacuum-level depressurization. These maximum temperatures are also seen to be only weakly dependent on J. Additionally, as will be shown later from flash experiments using a custom vapor chamber, flash is observed for liquid methanol at room temperature and depressurized to soft vacuum (Fig 4.5.6). So, while experimental temperature conditions are inconsistent with the aforementioned temperatures obtained theoretically, such theoretical values give the maximum liquid superheat temperatures. Furthermore, perturbations to the system, especially those introduced by the depressurization wave and the presence of micro bubbles of dissolved gas, act to significantly reduce the incipient temperature for nucleation.

Another approach to incipient nucleation can be obtained by Hsu's criteria [2.2.2] for heterogeneous nucleation. The governing equation is shown below with the corresponding incipient superheat shown as the left-hand side of Eqn. (2).

$$T_l - T_{sat} = \left[\frac{2C_2\sigma T_{sat}q}{\rho_v h_{fg} k_l}\right]^{\frac{1}{2}} \tag{2}$$

where $C_2 = 1 + \cos\theta$ and θ is contact angle between liquid and wall surface, σ is surface tension (N/m), T_{sat} is saturation temperature corresponding to system pressure (K), q is applied heat flux at the wall (W/m^2), ρ_v is vapor density (kg/m^3), h_{fg} is heat of vaporization (kJ/kg), and k_l is thermal conductivity of the liquid (W/(m · K)).

The absolute pressure necessary for heterogeneous nucleation is shown below as a function of liquid methanol temperature. For simplicity, q is assumed to equal 10 kW/m^2 and C_2 is assumed to equal 1.

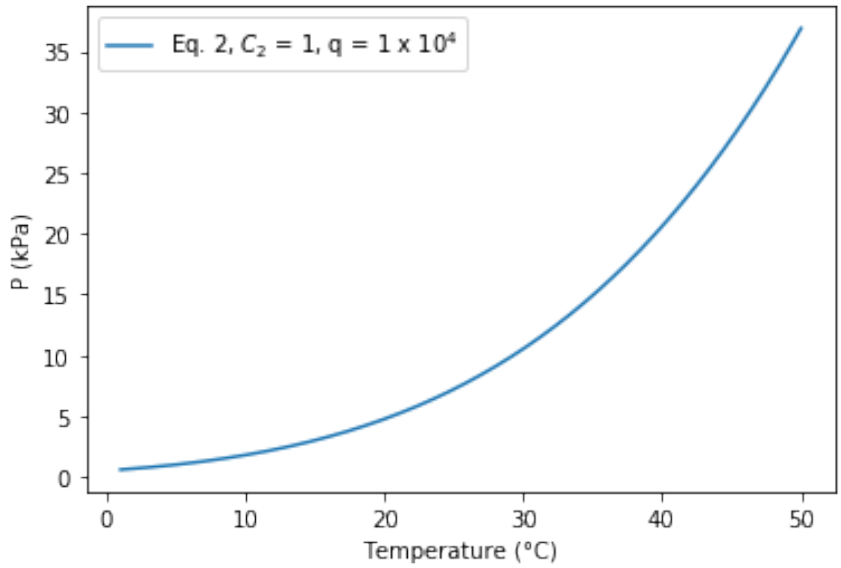

Fig. 2.2.2: Vacuum pressure requirement for heterogeneous boiling for various liquid methanol temperatures.

From Fig. 2.2.2, for methanol initially at room temperature, the absolute pressure required for heterogeneous nucleation assuming a heat flux value of 1W/m^2 and contact angle of 90 degrees is about 18 kPa. This result is compatible with similar vacuum levels (18 – 20 kPa, absolute) experimentally applied for methanol initially at room temperature to flash. However, we need to proceed with caution, as the assumed heat flux value is not representative of actual heat loads.

A more general superheat incipience, based on cavity size [2.2.1], can be expressed as:

$$T_l - T_{sat} = \frac{4\sigma T_{sat}}{\rho_v h_{fg} D_c} \tag{3}$$

where D_c is nucleating cavity mouth diameter. Noting that this expression is independent of heat flux, and converting a temperature difference to a pressure difference, the relation between pressure reduction and nucleating cavity mouth diameter is plotted in Fig. 2.2.3 for a variety of liquid temperatures, assuming the initial state of the working fluid is saturated liquid. This assumption is necessary since a corresponding pressure is required for T_l.

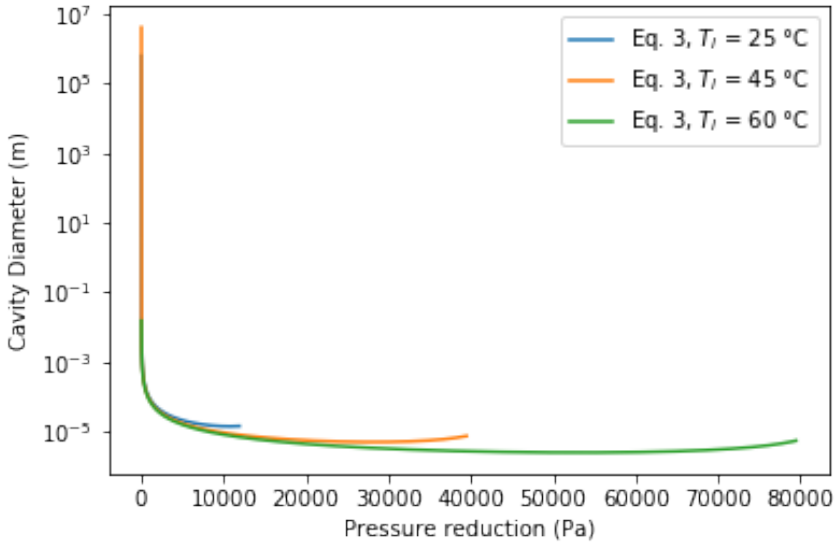

Fig. 2.2.3: Nucleating cavity diameter as a function of pressure reduction for various initial liquid temperatures.

The smallest cavities, from a temperature-controlled nucleation standpoint, require the highest superheat to nucleate. From Fig. 2.2.3, the absolute minimum for each curve corresponds to the smallest nucleating cavity, which require only a partial depressurization to nucleate. For example, for the $T_l = 60$℃ case (near saturation temperature for 1 atm pressure), a cavity diameter of 2.5 μm can nucleate for a pressure reduction of 53000 Pa. Assuming that actual cavity diameters are about equal to surface roughness, which is about $1 - 10$ μm for unpolished surfaces, this model suggests that an unpolished chamber, initially filled with methanol and heated to 60℃,

should produce boiling at a pressure reduction of about half vacuum. Evidence of boiling can be determined by measuring the local temperature of the chamber, which would decrease as a result of the fluid phase change. However, in relation to heterogeneous nucleation, this model assumes bubble growth at a wall, and the effect of dissolved gas is not considered, which can significantly lower inception superheat and thus the pressure reduction needed for onset of flash.

The previous figures in this chapter consider boiling from a wall heat flux, temperature-driven, surface cavity nucleation. The goals of such models were to convert the governing equations such that temperature differences are converted into pressure differences as a first approximation of understanding flash boiling as a pressure-driven process. However, in doing so, the assumption of flash boiling as a volumetric phenomenon is overlooked. Better models are needed to capture the dynamics of flash while staying faithful to physical principles underlying the rapid flash process.

By understanding the main factors that affect the initial stages of flash, an engineering model can extract parameters needed for controlling flash boiling in a flash vapor chamber. This project aims to demonstrate transient cooling performance of an open-loop flash vapor chamber architecture upon heating and provide an interpretive model for flash discharge based on thermodynamic theory, real fluid properties, and empirical data. First, we highlight important factors that influence bubble nucleation.

2.3 Pressure undershoot

As boiling depends on thermophysical conditions both spatially and temporally, the local system pressure plays an important role in determining saturation conditions. Pressure is not a static quantity, but a dynamic one that only changes with time and location during a flash process, as pressure waves propagate once a system is initially depressurized to initiate flash boiling. Here, background on pressure wave propagation is presented. As a pressure wave traverses, for instance through a tube, it was observed that at the location at the far end of the tube away from the surface

closest to the initial depressurization the local pressure briefly dropped to a value below that prescribed by the initial depressurization. This phenomenon is denoted as pressure undershoot, and an example of pressure undershoot in a tube is shown below.

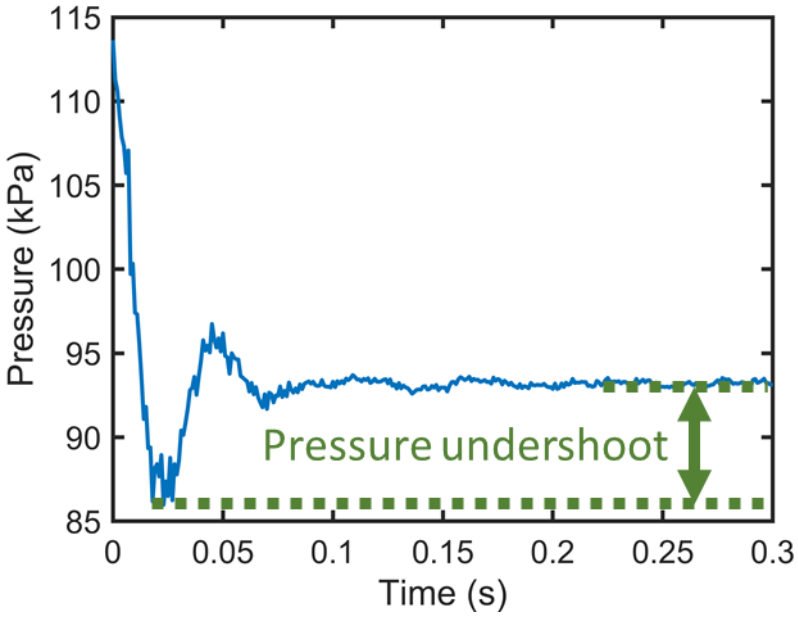

Fig. 2.3.1: Definition of pressure undershoot.

This undershoot phenomenon, as a result of the reflected pressure wave at the end of the tube, has also been observed experimentally in prior work. Miyazaki et al. demonstrate reported pressure undershoots of up to 50% for an air-water mixture in a 2.1 m long vertical tube [1.3.14].

This phenomenon has some important implications. Firstly, if local pressure within a system can achieve a minimum at a specified location, then localized flash boiling becomes possible. Also, the presence of the pressure undershoot reinforces the idea that only a partial initial depressurization is needed for flash; the undershoot will deliver a further local reduction in pressure that brings the working fluid to conditions suitable for bubble nucleation.

2.4 Dissolved gas

Another important aspect that affects the conditions necessary for nucleation is the presence of dissolved gases in the working fluid prior to flash. Dissolved gases influence the onset

of boiling by lowering the inception superheat. Müller-Steinhagen et al. reported that the type of dissolved gas can significantly affect onset of nucleation, e.g., inclusion of dissolved propane in heptane reduced the incipient bubble formation temperature from 90.5°C to 3.5°C [2.4.1].

As such, we hope to promote boiling by introducing dissolved gas, either passively or actively. A passive solution would be to have a working fluid reservoir in which gas is dissolved prior to cooling. An active solution can be one in which gas bubbles can be introduced to the system near the heat source and intelligently timed with the depressurization such that the superheat requirement for boiling is lowest for the location of interest, thereby aiding bubble nucleation and growth for flash boiling. For experiments conducted in this work, a passive approach is used, and effects of dissolved gas are analyzed in section 4.7.3 by comparing flash efficacy of degassed and aerated methanol.

Chapter 3: Experimental characterization of pressure wave propagation and flash incipience

3.1 Background

We consider the gaps in knowledge between traditional thermally-driven boiling and pressure-driven flash boiling as motivation for our experimental studies. Traditional boiling and related phase-change heat transfer processes use heat input to drive bubble growth, nucleation, and departure at constant pressure. When boiling is thermally driven, the temperature becomes a dependent variable that responds and adjusts to the loading conditions, conflicting with many practical engineering needs since temperature also serves as a primary performance metric and objective function in thermal management.

We recognize that, as a pressure-controlled boiling phenomenon, flash boiling, or the inception thereof, is sensitive to the pressure-controlled local liquid superheat. To better understand the underlying physical processes that drive flash discharge so a predictive model for flash can be implemented in real systems, we address the superheat criterion for nucleation. The goal of our experiments is to provide insight into flash incipience conditions so that models for flash cooling can be developed.

The efficacy of flash for transient cooling can be understood by considering the general conditions required for phase-change heat transfer. In thermally-driven boiling, liquid must be heated to (and beyond, i.e., superheated) the saturation temperature corresponding to the system pressure. Experimental investigation of the nature of pressure wave propagation offers insights about both the spatial and temporal aspects of bubble nucleation as it pertains to pressure undershoot. Pressure undershoot has some important implications, especially considering that if local pressure within a system can achieve a minimum at a specified location, then localized flash boiling becomes possible. Since pressure undershoot has been shown to be quite considerable,

only a partial depressurization is needed such that conditions at the far end of the system are conducive for boiling. As such, the nature of pressure wave propagation is first investigated, followed by depressurization required for flash inception.

3.2 Experimental methodology for pressure wave propagation

The experimental setup to conduct pressure wave propagation measurements is similar to that of Miyazaki et al. [1.3.14]. A long, vertical copper tube is filled with methanol and subject to various depressurizations, whose magnitudes are captured with pressure gauges placed at the top and bottom of the tube. Thermocouples are also placed on the outside of the tube to measure changes in temperature associated with flash. The schematic for the experimental setup and the actual setup are shown as follows. Further details about the setup are presented in section A.2.

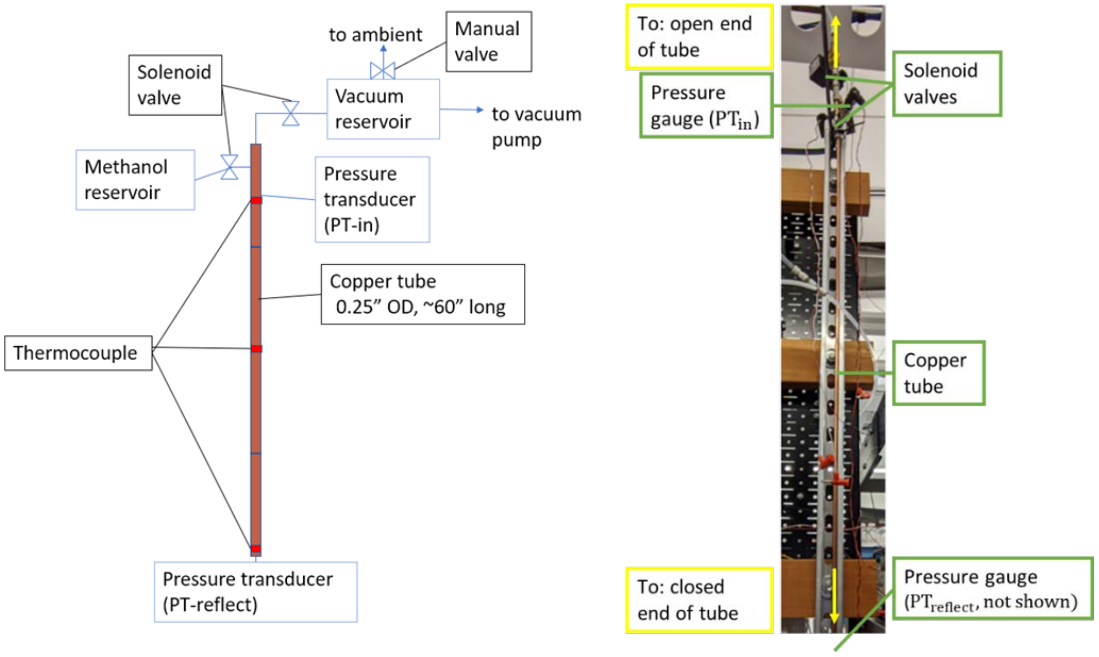

Fig. 3.2.1: Pressure wave propagation experimental setup, with sensors comprised of: OMEGA SA1-K surface thermocouples and OMEGA PX-119-015AI pressure transducers.

3.3 Results for pressure wave propagation

Data obtained from the experimental setup for various depressurizations are shown. Since pressure undershoot was previously demonstrated by Miyazaki to be maximum for the far tube location away from the initial depressurization, data for PT-reflect is of interest more than PT-in.

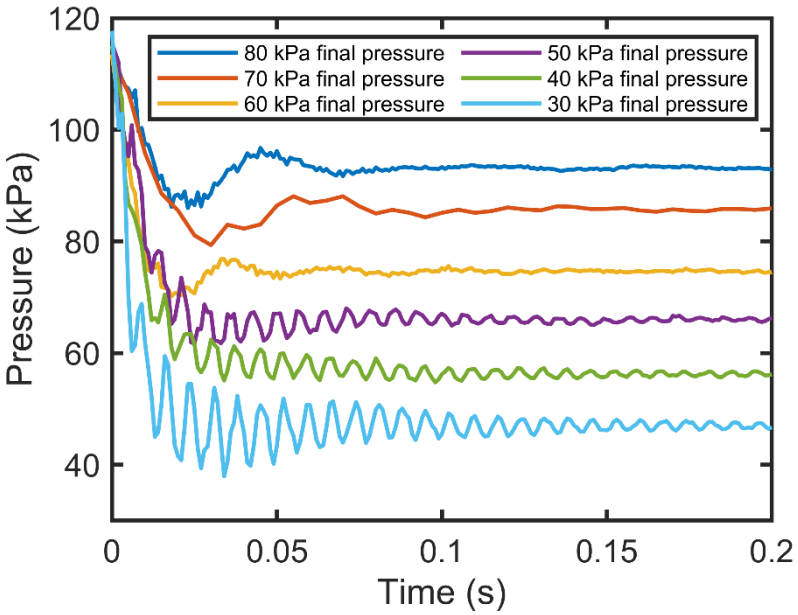

Fig. 3.3.1: Average PT-reflect pressures as functions of time for various prescribed final pressures.

Pressure undershoot is observed to occur within 0.05 s for all depressurizations, with higher final prescribed pressures displaying local pressure maxima after the initial depressurization that become less pronounced with decreases in final pressure. However, for low final pressures, secondary resonance-like behavior is observed. The frequency of these resonant oscillations is calculated to be 139 Hz. The data corresponding to all test trials is represented in the following scatterplot.

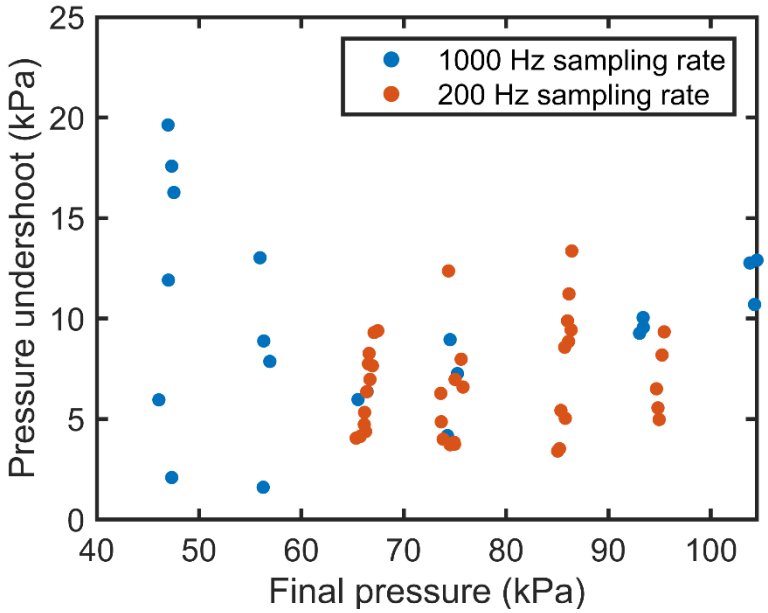

Fig. 3.3.2: Scatterplot of pressure undershoot as a function of depressurization pressure.

Here, the goal was to observe relations between pressure undershoot and final prescribed pressure, but Fig. 3.3.2 shows that the data have wide variability, especially for low final pressures. No clear relation between undershoot and final pressure is apparent, but further testing is needed, especially for lower pressures close to the saturation pressure for methanol at standard temperature.

From Fig. 3.3.1, there is an increase in high-frequency oscillations with decrease in final pressure. For analysis, a spectral decomposition of the 30, 40, and 50 kPa data is performed using a Fast Fourier Transform (FFT). The results are shown in Fig. 3.3.3.

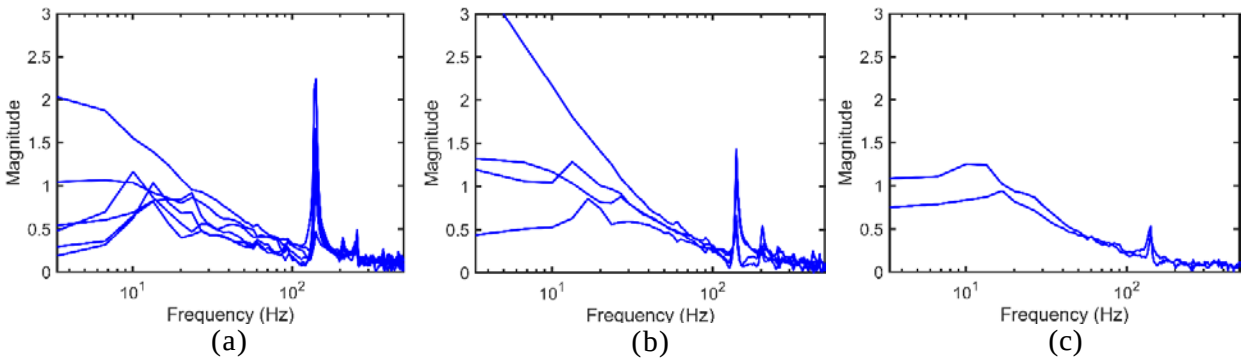

Fig. 3.3.3: FFT of $PT_{reflect}$ *for selected data. (a) 30 kPa vacuum reservoir. (b) 40 kPa vacuum reservoir. (c) 50 kPa vacuum reservoir.*

For low vacuum reservoir levels, a pronounced vibrational effect around 140 Hz is observed. The 30 kPa data are further analyzed below.

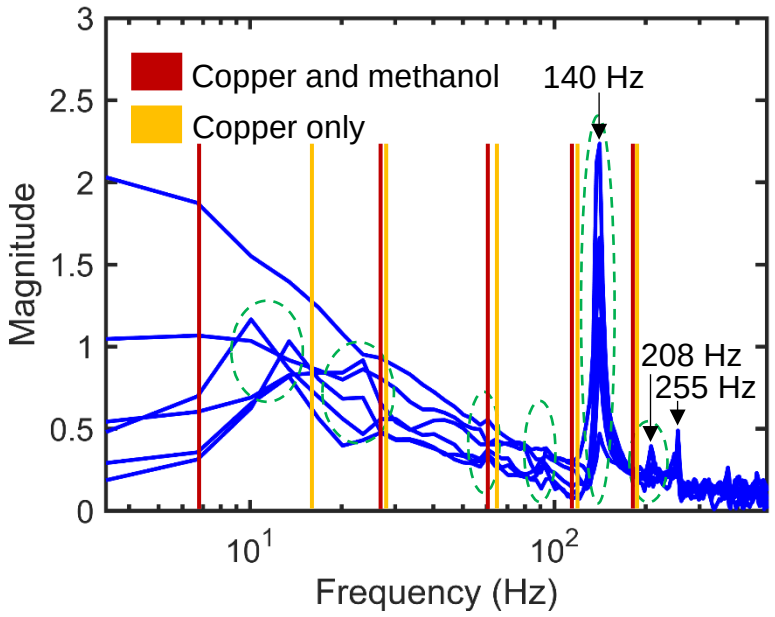

Fig. 3.3.4: Comparison of FFT of $PT_{reflect}$ *with tube resonant frequencies for 30 kPa vacuum reservoir.*

Here, frequencies corresponding to the natural resonant frequencies of a copper and combined copper and methanol tube are shown by the vertical yellow and red lines, respectively

[3.3.1]. Resonant frequencies for the tube are calculated assuming a straight beam hinged at both ends under zero axial tension. In Fig. 3.3.4, the areas labeled green (corresponding to local maxima in the FFT) lie close to the calculated vibrational modes of the tube, so there is evidence to support the notion that both tube geometry and tube material affect the overall pressure propagation.

3.4 Experimental methodology for flash incipience

Next, additional experiments were carried out with the long tube setup to understand the role of orientation for pressure wave propagation during flash. To aid in flash initiation, the tube was heated to a desired steady-state initial temperature before depressurization to increase the liquid superheat of the methanol inside the tube after depressurization. The test setup is shown as follows:

Fig. 3.4.1: Horizontal tube setup for pressure wave propagation experiments.

For these experiments, the $PT_{reflect}$ vacuum gauge would break if the vacuum reservoir pressure was too low. Thus, 40 kPa was set as the lowest limit, and the initial temperature was chosen such that the liquid methanol would be superheated upon depressurization; that is has a temperature higher than that corresponding to saturation at the vacuum reservoir pressure.

3.5 Results for flash incipience

Results were obtained for calculated superheats of 5°C and 13°C. While care was taken to ensure temperature uniformity throughout the tube, the resistive heating wire used to heat the tube was wrapped around the middle thermocouple, leading to higher temperature measurements than expected at the middle of the tube. The initial temperature is therefore taken as the average of the temperatures measured by the top and bottom thermocouples.

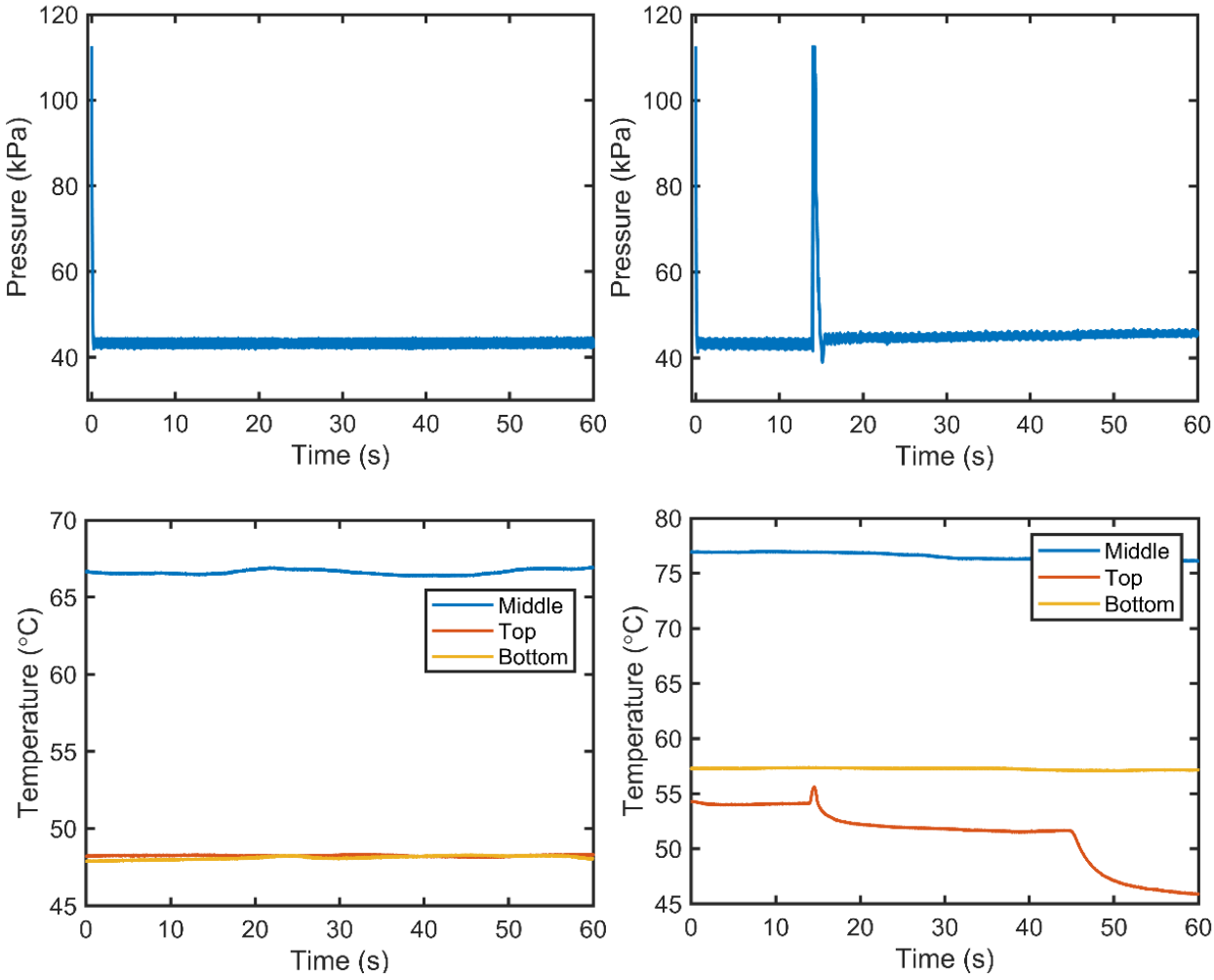

Fig. 3.5.1: Internal tube pressure measurements and external temperature measurements for horizontal tube pressure wave propagation experiments. (a) initial temperature: 48°C (est.), vacuum pressure: 40 kPa. (b) initial temperature: 56°C (est.), vacuum pressure: 40 kPa.

For the case with 5°C superheat shown on the left of Fig. 3.5.1, there was no noticeable temperature decrease following depressurization, so there was no evidence of flash for this configuration. However, for the case with 13°C shown on the right, a pressure spike occurs at around 14 s that is evident of vapor generation during flash, which is also corroborated by exponential temperature decrease characteristic of flash; therefore, we conclude that flash occurred for this configuration, albeit delayed from the initial depressurization. This result seems to indicate that, at least for the horizontal tube configuration, a moderate inception superheat must be met for the methanol to flash.

To further add to the comparison of the thermophysical characteristics during depressurization for various orientations, a similar set of experiments was performed using the long tube in a *vertical* orientation. By doing this, the effects of 1g on flash boiling can be studied. The results are shown as follows.

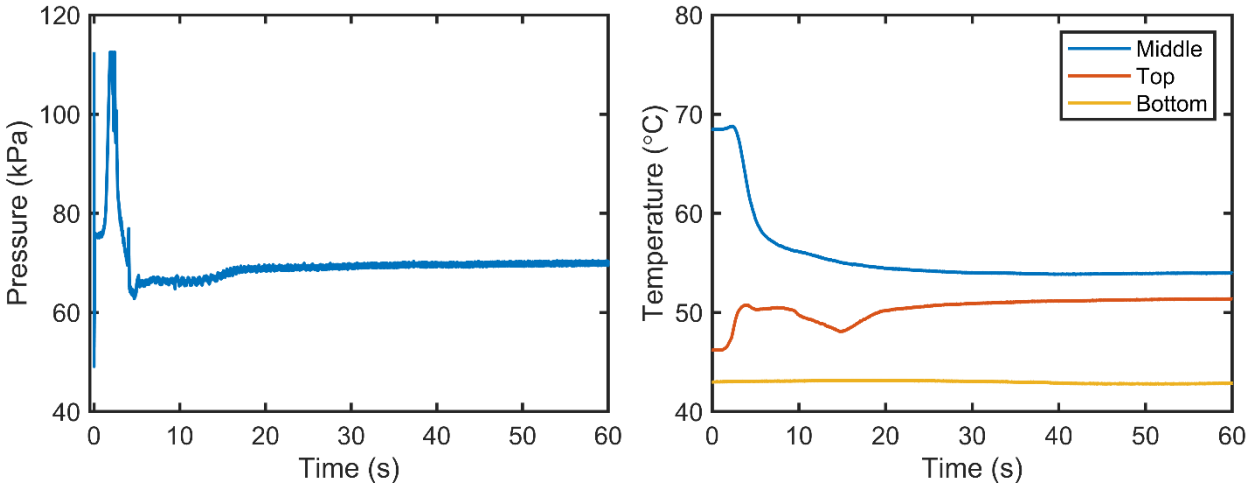

Fig. 3.5.2: Internal tube pressure measurements and external temperature measurements for vertical tube pressure wave propagation experiments. Initial temperature: 44°C (est.), vacuum pressure: 60 kPa.

A somewhat surprising result is shown. In this experiment, the saturation temperature for methanol at the vacuum reservoir pressure of 60 kPa is 52°C, and the initial steady state temperature of the methanol in the tube prior to depressurization is about 44°C. The liquid is not superheated, and even not saturated for the conditions after depressurization, but the pressure spike at 4s and the temperature drop measured by the middle thermocouple indicate evidence of vaporization inside the tube. A close look at the pressure graph reveals a pressure minimum of 49 kPa, for which the corresponding saturation temperature is 47°C. While the estimated initial temperature falls short of saturation conditions, the flash effect could be due to dissolved gas, which would reduce the saturation temperature. Even with this peculiarity, by comparing the inception superheat for the vertical tube and that of the horizontal tube, there is evidence that for a strong dependence on orientation for flash efficacy. Furthermore, the pressure undershoot is the driving mechanism for promoting conditions conducive for flash onset, and evidence shown above further corroborates the importance of pressure undershoot, and hence pressure wave propagation, on boiling inception.

Chapter 4: Flash vapor chamber cooling

4.1 Background

In this chapter, we consider transient cooling of a vapor chamber for practical assessment of flash efficacy. Vapor chambers have become an integral part of many electronic systems including aerospace components for steady-state high-heat-flux conditions. However, many applications (e.g., high-power radar) are either operated for a brief time or require high initial transient cooling before operating at steady state. In such cases, conventionally, an overdesign approach is used with a steady-state cooling solution matched to peak heat fluxes. However, a more efficient and compact design would use an adaptive approach that can support these high transients briefly without extraneous steady-state operation. One such application is demonstrated here for flashing in a vapor chamber, and the transient cooling phenomenon as a result of flash boiling is what we show in our experimental studies.

For the experiments, a commercial vapor chamber was used and a thermo/fluid network with thermocouple and pressure gauges was constructed to control and monitor fluid flow within the open-loop system. A schematic of the setup and corresponding Piping and Instrumentation Diagram (P&ID) is shown in Fig. 4.2.1. An idealized closed-loop cycle is also shown, which is used later to show regions of interest for each experimental study. Here, we demonstrate flash cooling processes that use pressure to control boiling heat transfer in an open system to achieve on-demand rates of heat transfer with targeted operating temperatures. Subsequent sections address gaps in knowledge arising from the inadequacy of temperature-driven approaches to flash modeling, and the transition difficulty from single bubble dynamics/heat transfer to system level heat transfer performance. This pressure-driven boiling approach can provide rapid, transient cooling at specific temperatures (including sub-ambient) with active control.

4.2 Experimental methodology

The testing conditions for this setup primarily focus on flash vapor chamber cooling for two different heat loading conditions. The first heat loading condition consists of a constant heat load (used to achieve steady-state initial conditions in the vapor chamber prior to flashing) that is maintained before and after flash initiation. These circumstances correspond to an initial low level of heating that is spread throughout the vapor chamber without increasing the fluid temperature beyond its boiling point, followed by a flash event that promotes rapid phase change. The second heat loading condition consists of a step-change in heat load applied simultaneously with flash initiation, hereafter denoted as a step heat load. For this case, flash initiation and change in heat load are applied after steady-state initial conditions in the vapor chamber are met. These circumstances correspond to impulsive, transient heat loads. Fig. 4.3.1 and Fig. 4.3.4 provide context for flashing with a constant heat load and flashing with step heat loads, respectively.

To help quantify flash cooling rate, the temperature of the vapor chamber was averaged over two thermocouples: one placed on the top side of the vapor chamber near the discharge port, and one placed on the bottom side, towards the edge, as shown with the magnified inset view in Fig. 4.2.1. The initial equilibrium setting was achieved by ensuring a temperature drift of no more than 0.2 °C/min for a given heat load. Primary variables of interest include (1) the amount of working fluid, expressed as a filling ratio, which is defined as the volume of liquid methanol divided by the volume of the internal volume of the vapor chamber, and (2) initial temperature. Further details about this setup can be found in section A.3.

To conduct experiments, the chamber is first evacuated to soft vacuum with the help of the vacuum pump. Afterwards, a specific amount of methanol is introduced using the injection syringe as shown in Fig. 4.2.1. Brief perturbation on the exterior of the vapor chamber is necessary to minimize liquid deposition within the dead volume inside the tubing. Heat was then applied to

the bottom of the vapor chamber to create elevated steady-state temperature conditions with minimal temperature drift. During the heating process, a ball valve connected to the open ambient is periodically controlled to maintain an internal pressure of 101 kPa. At steady state, the solenoid valve connected to the accumulator is opened, allowing flashing to begin.

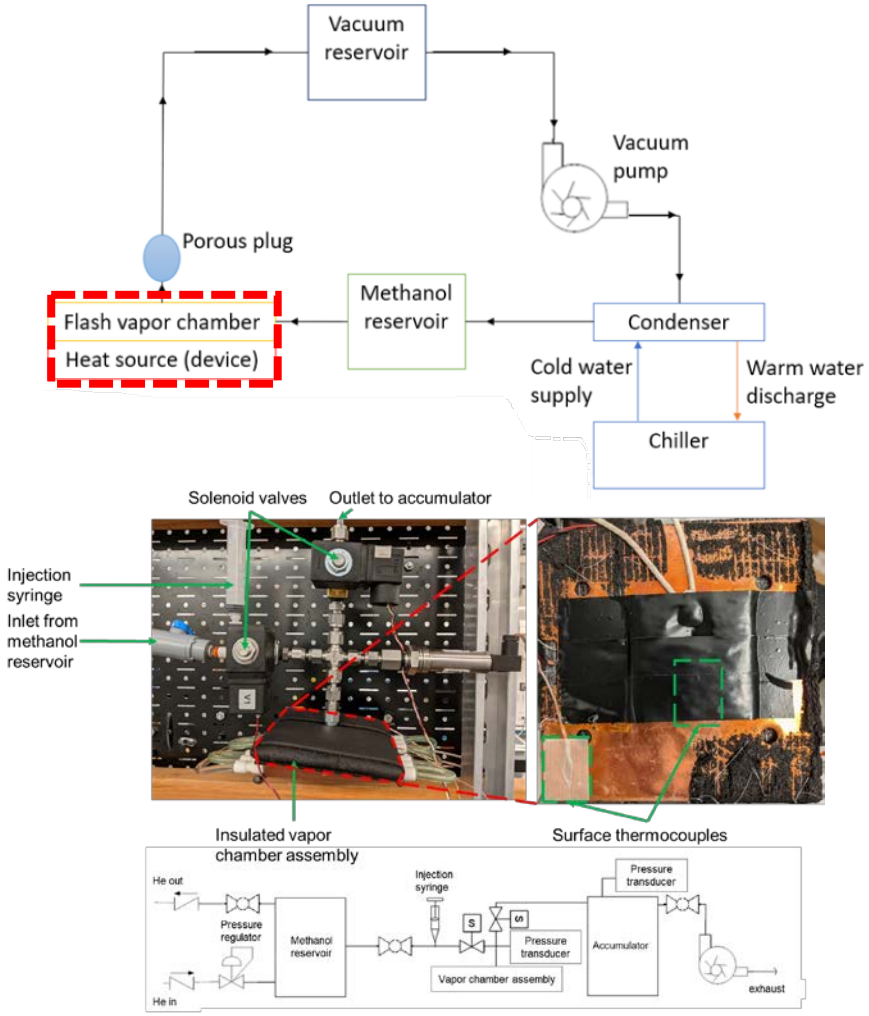

Fig. 4.2.1 Schematic and P&ID of experimental flash vapor chamber setup.

4.3 Results for flash incipience in vapor chamber

Flash onset can be used to characterize fluid state during flash. Experimentally, flash onset is determined by a local rise in pressure following depressurization. From these empirical

measurements, equivalent flash inception superheats are plotted for cases of flash cooling under constant heating and transient step heating, shown in Fig. 4.3.3. and Fig. 4.3.6, respectively.

4.3.1 Flash incipience under a constant heat load

Local pressure inside the vapor chamber is shown in Fig. 4.3.1 for representative data, in which the sharp drop in pressure is caused by opening of the valve connecting the vapor chamber to the vacuum reservoir, and corresponding periods of pressure increases due to vaporization are circled.

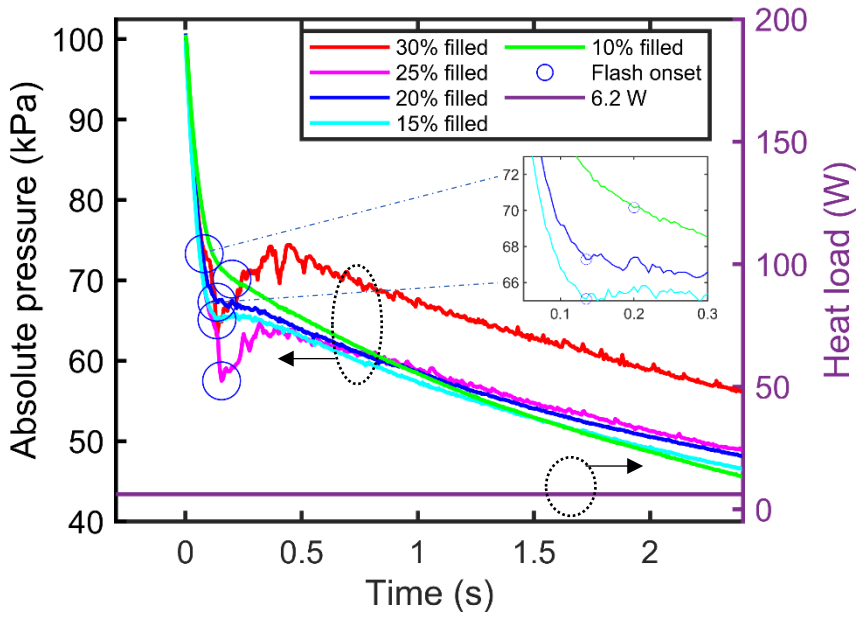

Fig. 4.3.1: Vapor chamber pressure and heat load as functions of time during flash for various filling ratios under constant 6.2 W heating, with flash onsets circled.

With the onset of flash determined from pressure measurements, the incipience of flash can be prescribed in terms of temperature by using analogous liquid superheats. Doing so allows for flash boiling, a pressure-controlled phenomenon, to be compared to traditional thermally controlled boiling processes.

First, the experimental flash onsets are compared to the saturation pressures corresponding to the initial steady-state temperature before flash, shown in Fig. 4.3.2. While the experiments were conducted under constant heating conditions, variability in the ambient environment led to temperature variations between 56.5°C and 59.5°C. Nonetheless, each experimentally-derived flash onset falls below the corresponding saturation pressure, supporting the notion that the liquid methanol is adequately depressurized for phase-change to occur. To express flash inception in terms of liquid superheat, the difference between the initial liquid temperature and the saturation temperature corresponding to the flash onset pressure is plotted in Fig. 4.3.3.

The results in Fig. 4.3.3 indicate that flash boiling has low superheats characteristic of heterogeneous boiling. Keeping in mind that flash boiling is a volumetric phenomenon, it retains the qualities of homogeneous boiling while only requiring liquid superheats characteristic of heterogeneous boiling. This characteristic of flash was also observed in prior work [1.3.9].

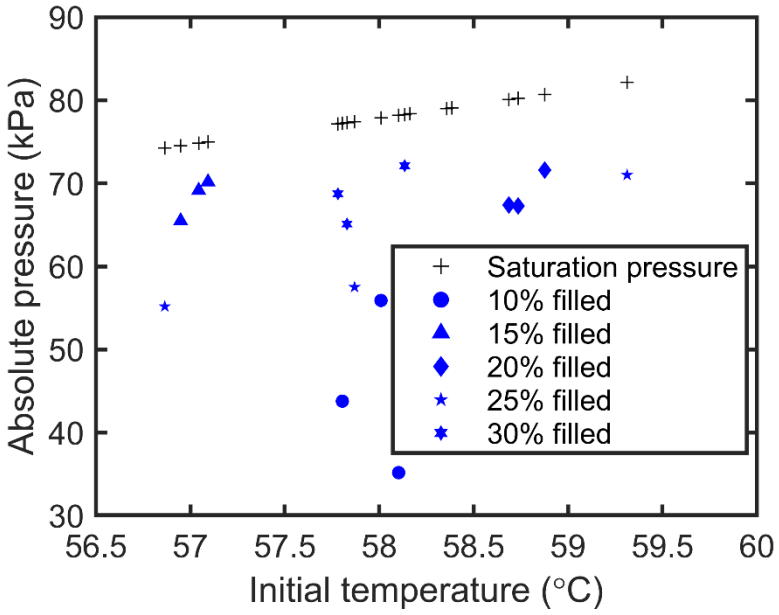

Fig. 4.3.2: *Experimental flash onset for various filling ratios under constant 6.2 W heating, with corresponding saturation pressures.*

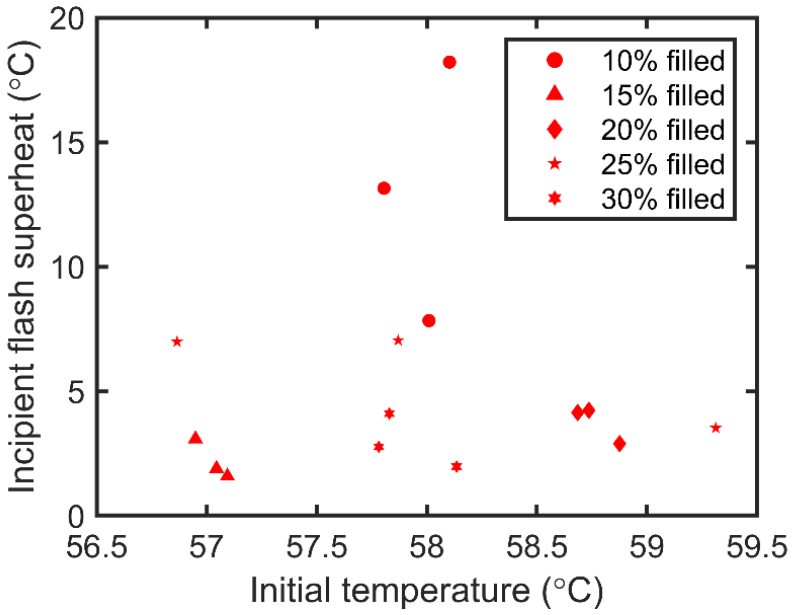

Fig. 4.3.3: Experimentally derived liquid superheats for flash inception at various filling ratios under constant 6.2 W heating.

4.3.2 Flash incipience under various step heat loads

For flash cases with step heating, the raw data for vapor chamber pressure during the first few moments of flash are shown in Fig. 4.3.4 for step heat loads of 45 W, 98 W, and 189 W, with circles indicating flash onset determined by the first measured increase in pressure. Additionally, the step heat loads of 45 W, 98 W, and 189 W are shown by the magnitudes of the step change in heating at $t = 0$. Prior to flash initiation, a heat load of 4.3 W was applied to achieve initial steady-state temperatures of about 61°C. (A lower heat load was required to achieve similar initial temperatures for those corresponding flash with various filing ratios because this experimental setup was better insulated). For these experiments, the filling ratio was kept constant at 20%.

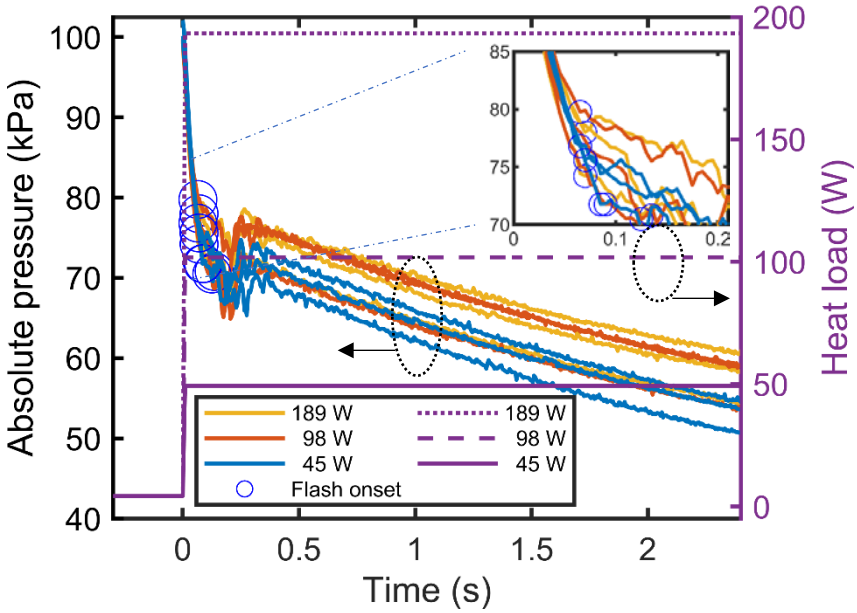

Fig. 4.3.4: Vapor chamber pressure and heat load as functions of time during flash for various step heat loads, with flash onsets circled.

From Fig. 4.3.1 and Fig. 4.3.4, the experimental flash onset occurs on a timescale of the order of 0.1 s. However, we proceed with caution as Fig. 4.7.6 and Fig. 4.7.2 in the proceeding sections indicate rapid vapor chamber cooling within 0.005 s, or about 20x faster. While the experimental flash onset is determined empirically, it is not without consideration of pressure buildup due to vaporization induced by sudden phase-change. However, the actual onset of bubble nucleation could be sooner, as pressure buildup due to vapor formation can result in a reduction in the initial rate of pressure decrease in the vapor chamber upon flash initiation, instead of a momentary pressure recovery as indicated with the blue circles in Fig. 4.3.4. Further experiments to more accurately determine vaporization onset would aid in better understanding thermophysical conditions necessary for flash. Nevertheless, the criteria used for experimental flash onset are useful in defining upper thresholds for incipient flash superheat, shown in Fig. 4.3.6.

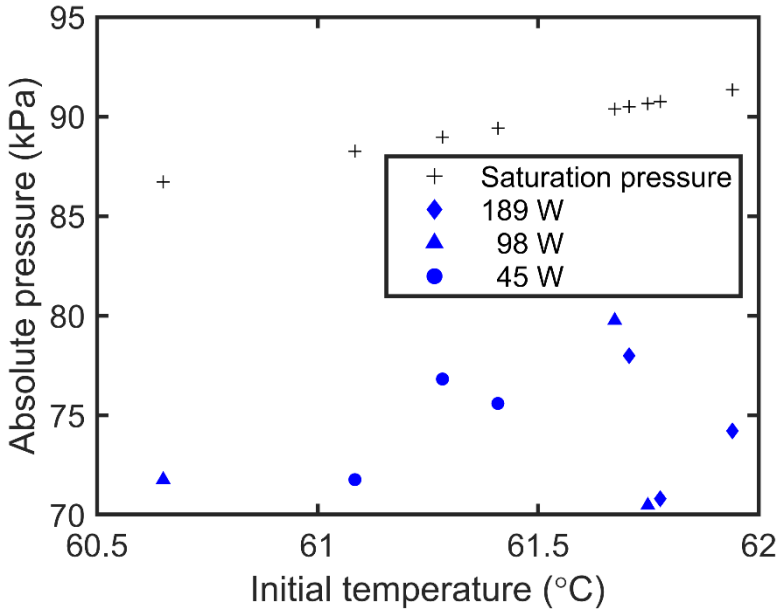

Fig. 4.3.5: Experimental flash onset for various step heat loads, with corresponding saturation pressures.

The changes in pressure are converted into superheats and plotted in Fig. 4.3.6. Comparing Fig. 4.3.6 and Fig. 4.3.3, no distinct change in mean incipient flash superheat due to the effect of step heating is apparent, but the plotted data variance is significantly reduced for the former. As discussed previously, these values represent the upper limit on inception superheat, as flash boiling can potentially begin at higher absolute pressures than the ones denoted in Fig. 4.3.5. Thus, superheat conditions necessary for flash boiling can be reasonably approximated as those corresponding of heterogeneous boiling.

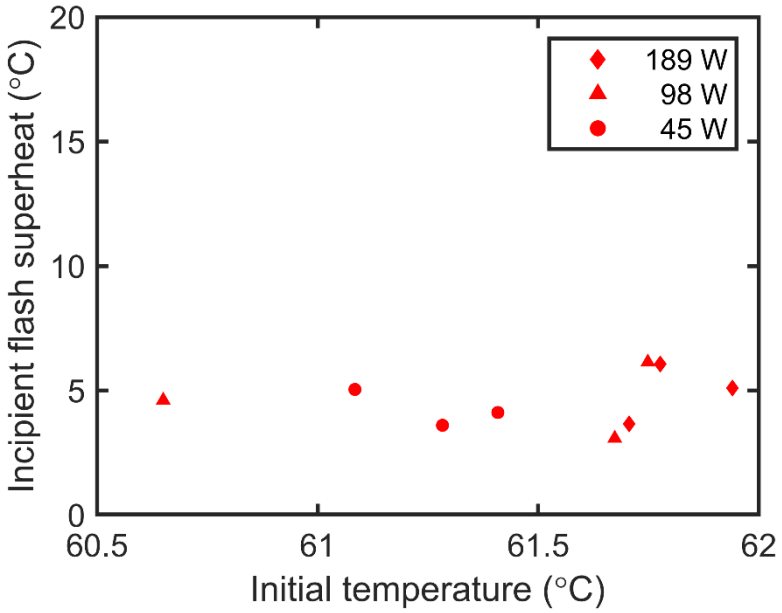

Fig. 4.3.6: Experimentally derived liquid superheats for flash inception at various step heat loads.

4.4 Approach to quantify flash vapor chamber cooling under constant heat loads

To provide an interpretive model to quantify flash behavior and performance, a lumped capacitance-based energy balance on the vapor chamber structure is performed. The governing equations follow and include contributions from heater input P(t), natural convection q_{nc}, radiation q_{rad}, and flash cooling q_{fc}.

$$\dot{E}_{in}(t) = \dot{E}_{st}(t) + \dot{E}_{out}(t) \tag{4}$$

$$P(t) = \dot{E}_{st}(t) + q_{nc}(t) + q_{rad}(t) + q_{fc}(t) \tag{5}$$

$$P(t) = \langle mC_p \rangle \frac{dT(t)}{dt} + \langle h_{ext} A \rangle (T(t) - T_a) + \langle \epsilon \sigma A \rangle (T(t)^4 - T_a^4) + q_{fc}(t) \tag{6}$$

In Eqn. (6), $T(t)$ is the temperature of the vapor chamber as a function of time, h_{ext} is the heat transfer coefficient between the exterior of the vapor chamber and the ambient environment, and T_a is the ambient room temperature (taken to be 25°C).

To simplify the analysis, a few assumptions are made. First, the heat transfer coefficient, h_{ext} is treated as a constant for each individual experimental run and depends only on the initial steady-state temperature for each experimental trial, heat load, and ambient room temperature. Second, it was initially assumed that radiation contribution is negligible. This assumption was justified in retrospect, since the heat loss from radiation is at most 2-3 W (compared to peak cooling rates above 60 W shown in Fig. 4.5.1 (b)) assuming an emissivity value of 1, i.e., a black surface. Thus, upon substitution of relevant properties, the final energy balance equation takes the following form:

$$P(t) = \langle m_{vapor\ chamber} C_{copper} \rangle \frac{dT(t)}{dt} + \langle h_{ext} A \rangle (T(t) - T_a) + q_{fc}(t) \tag{7}$$

Eqn. (7) is directly solved for q_{fc}, as all other quantities are either known or calculated from experimental data.

The theoretical maximum energy dissipation from flash boiling, E_{max}, is calculated based on the mass of methanol used, $m_{methanol}$, and the difference in enthalpy, Δh, between initial and final conditions. The initial enthalpy, h_f, is calculated based on initial steady-state conditions in the vapor chamber. The final enthalpy, h_g, is calculated using accumulator pressure and average temperature of the vapor chamber. This approach highlights the best-case scenario for a two-phase coolant to exchange heat with the chamber under specific experimental conditions at thermodynamic equilibrium. Thus, subsequently obtained efficiencies in Fig. 4.5.1 (d) are the limiting worst-case efficiencies for the flash pulses. The enthalpy calculations were performed with a MATLAB script accessing thermofluidic properties using the CoolProp database [4.4.1].

$$E_{max} = m_{methanol} \Delta h \tag{8}$$

The definition of cumulative efficiency, η, follows as the ratio of total cooling energy over a certain time interval, E_p, to the theoretical maximum:

$$\eta = \frac{E_p}{E_{max}} \tag{9}$$

where E_p is defined by integrating the flash cooling rate, as shown below.

$$E_p = \int_{t_i=0}^{t_f=t} q_{fc}(t)dt \tag{10}$$

4.5 Results and discussion for flash vapor chamber cooling under constant heat loads

The following results pertain to flash cooling of a vapor chamber that is initially at steady-state conditions. Parameters tested are: filling ratio, inclusion of a porous outflow plug, and initial liquid temperature.

4.5.1 Effect of filling ratio

The amount of liquid methanol in the vapor chamber was varied from 2.0 mL to 6.0 mL in these tests, and thus constitute filling ratios of 10% to 30%. Averaged data over several identical experiments for the change in vapor chamber temperature with constant heater input of 6.2 W are shown in Fig. 4.5.1(a). The exponential decay-like evolution of the change in temperature for the entire flash duration is also in agreement with prior work [4.5.1] [1.3.11] [1.3.12]. The internal methanol temperature was not directly measured; however, the methanol present in the vapor chamber after initial depressurization should exhibit a lower temperature than that of the outside of the vapor chamber. As a result of both the decrease in methanol temperature and the local pressure increase due to vapor generation, the liquid superheat is reduced, subduing the flashing phenomenon.

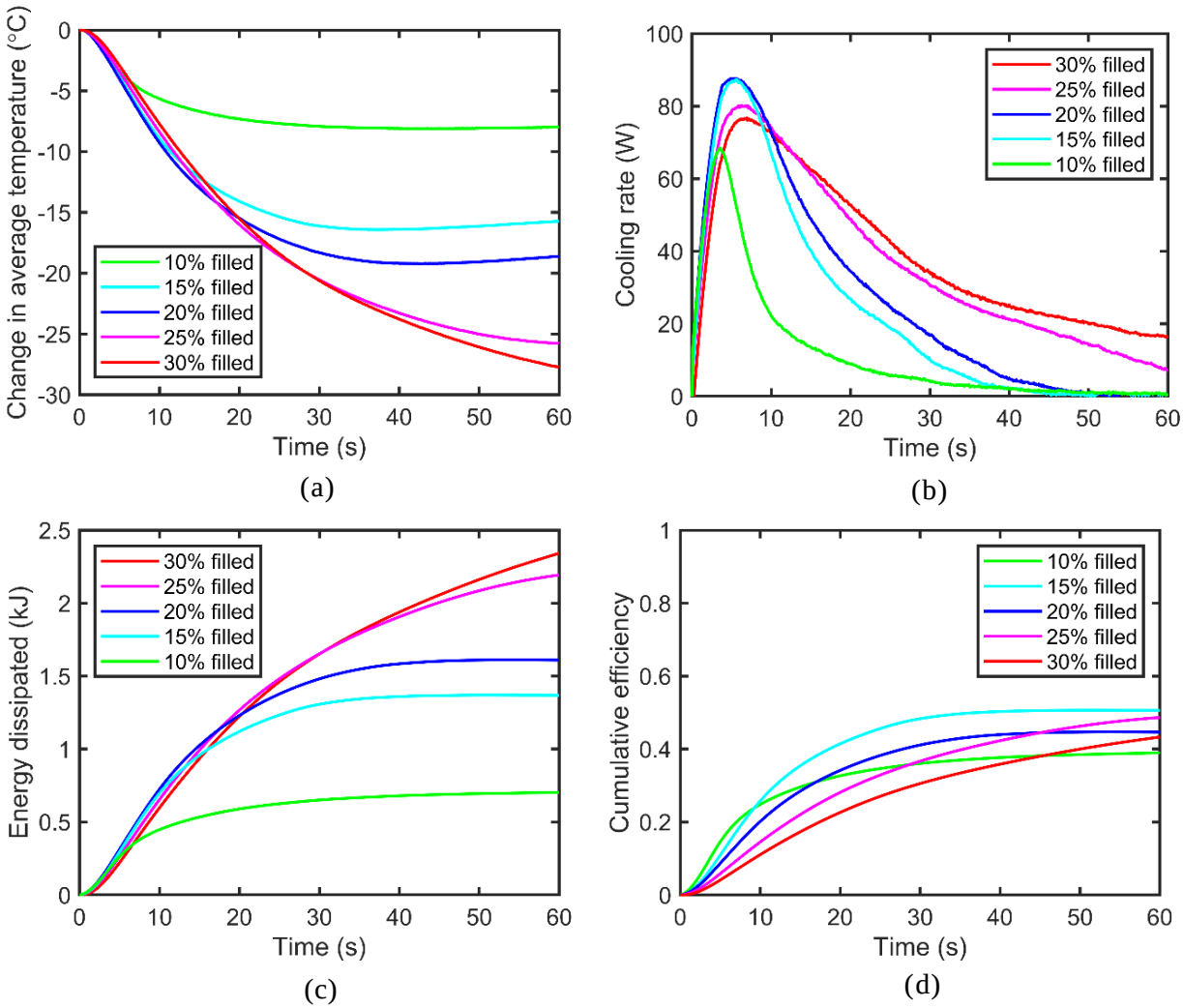

Fig. 4.5.1: Effect of filling ratio for constant 6.2 W heat load. (a) Change in average vapor chamber temperature as a function of time for different filling ratios. (b) Flash cooling rate, q_{fc}, as a function of time. (c) Cumulative energy dissipation, E_p, as a function of time. (d) Cumulative efficiency, η, as a function of time.

Additionally, as shown previously in Fig. 4.3.1, vapor generation during flash increases local pressure, thereby decreasing the rate of vaporization. The combined effect of decreased liquid temperature and increase in local pressure hinder the boiling process, causing a reduction of

cooling flux with time after peak cooling is reached. Additionally, at approximately 3 s after flash initiation, rate of temperature change is heavily influenced by filling ratio, as the transient cooling curves in Fig. 4.5.1(a) asymptote earlier for smaller filling ratios, signaling a shorter duration of cooling. The rapid, transient nature of flash cooling is illustrated in Fig. 4.5.1(b), as the cooling rate, $q_{fc}(t)$, is calculated from Eqn. (7) and processed temperature data. The cooling rate peaks early after depressurization, creating an initial peak. For cases of 10%, 15%, and 20% filling ratios, the onset of peak cooling rate is directly proportional to methanol amount. Maximum cooling rates for 10%, 15, and 20% filling ratios are attained at 3.6 s, 5.6 s, and 4.9 s, respectively. Fig. 4.5.2 shows the existence of an optimal filling ratio to be between 15% and 20%.

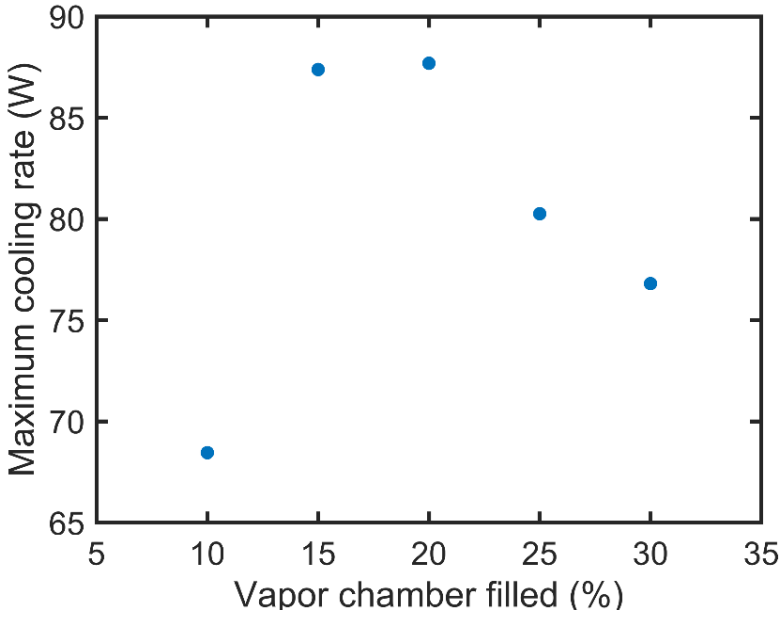

Fig. 4.5.2: Peak flash cooling rate, $q_{fc,max}$, attained as a function of vapor chamber filling.

After peak cooling, all cooling rates decay to zero, signaling the complete vaporization of methanol present in the vapor chamber. We observe that for the case of 25% vapor chamber filling, the trend of increases in both cooling rate and onset of peak cooling with methanol amount

is no longer followed, demonstrating adverse effects of excess working fluid on cooling performance.

The total energy dissipated over time by a single pulse for different cases is shown in Fig. 4.5.1(c). The cumulative efficiency over time is shown in Fig. 4.5.1(d) and is calculated by evaluating Eqn. (9) at every time step. The cumulative efficiency curve for 30% vapor chamber filling shows how additional methanol present in the vapor chamber acts as a diminishing return- while an increase in filling ratio allows for prolonged boiling and thus prolonged cumulative cooling, it is at the expense of a decrease in peak cooling rate.

4.5.2 Effect of inclusion of a porous outflow plug

Another consideration studied is the effect of a porous outflow plug, highlighted in red as shown in the following schematic.

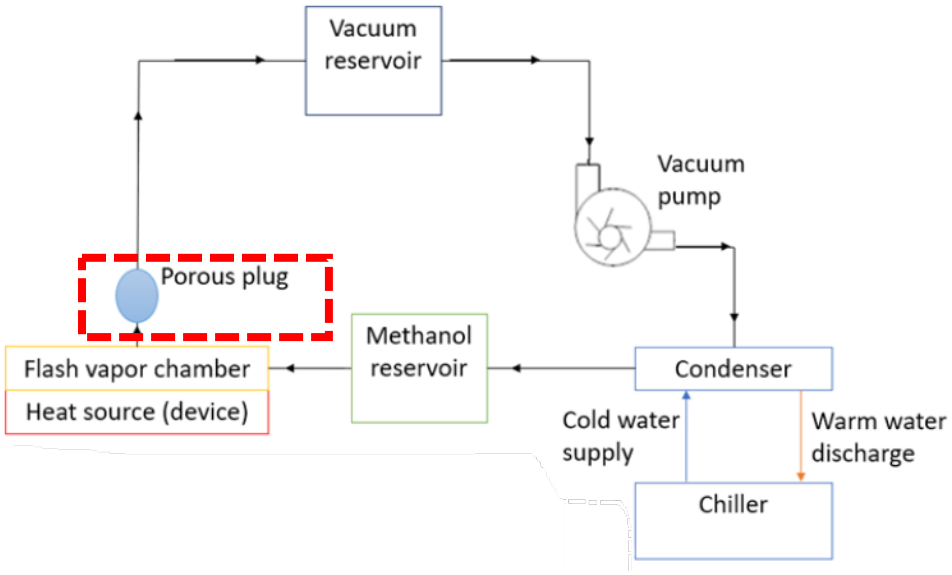

Fig. 4.5.3: Schematic showing relative location of porous outflow plug.

In the foregoing results and corresponding experiments, premature discharge of liquid methanol out of the vapor chamber during flash was observed. Ideally, the methanol remains inside the vapor chamber during the flash process so that cooling is localized within the vapor

chamber and as close to the heat source as possible. With the goal of retaining liquid inside the vapor chamber in mind, it was postulated that addition of a porous plug at the outlet of the vapor chamber would serve to better contain the liquid and hinder it from escaping the vapor chamber. The porous plug used for testing was steel wool, compacted to fit snugly inside the outlet of the vapor chamber.

Experiments performed with the porous plug were conducted in a similar manner to those without it, and the results are shown comparing the effect of the porous plug for various vapor chamber filling ratios under a constant heat load of 6.2 W. Only one experiment was done for each filling ratio due to experimental difficulties; future work should take additional data to corroborate these findings.

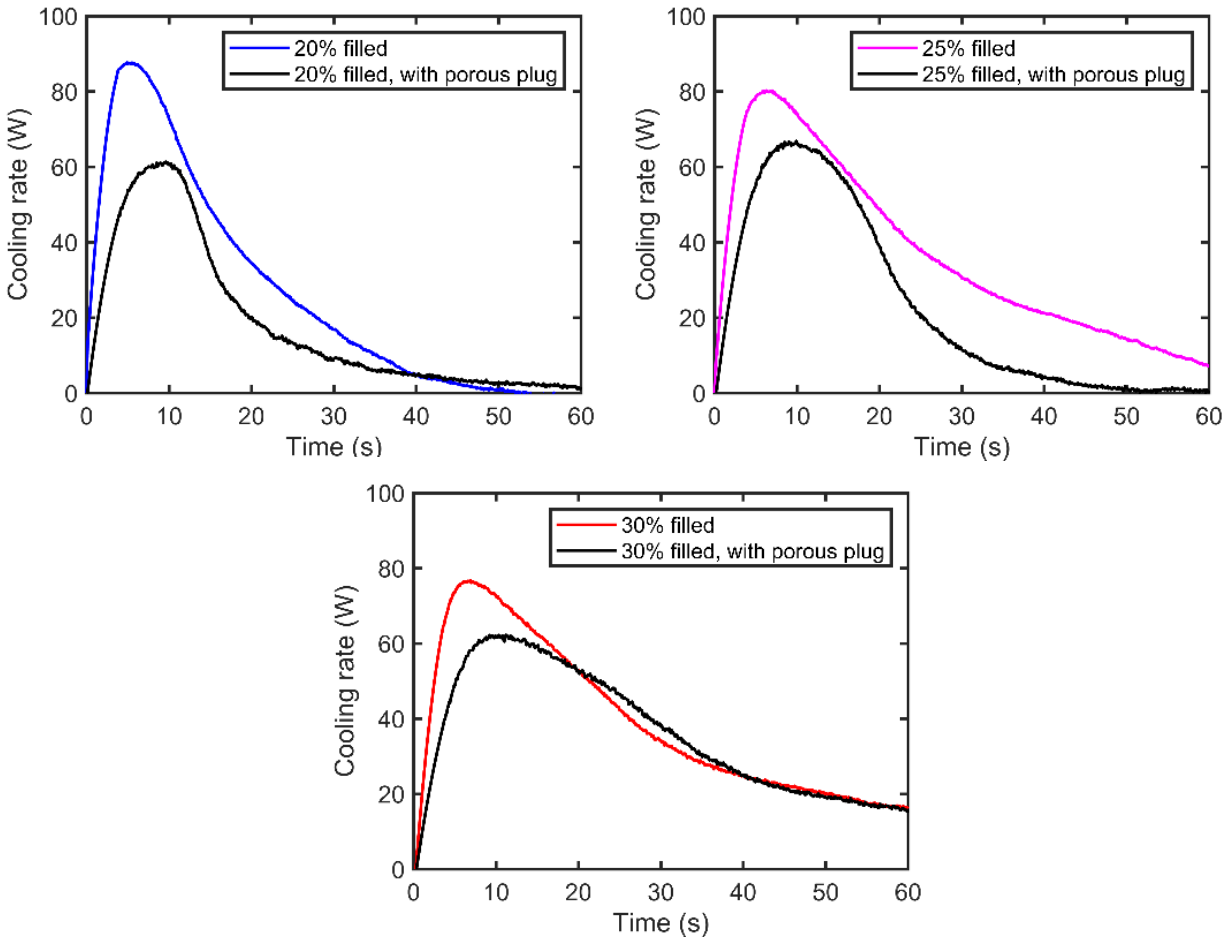

Fig. 4.5.4: Effect of porous plug on flash cooling rate, q_{fc}, for various vapor chamber fillings and constant 6.2 W heating.

From Fig. 4.5.4, peak cooling is reduced when the porous plug is present. Interestingly, however, the duration of near-peak cooling is increased, as shown by the broadening of the peaks in black. This increase in duration of near-peak cooling can be attributed to the liquid retention in the vapor chamber during flash, which is corroborated by visual confirmation during experimentation that less methanol was visible in the plastic vapor chamber outlet tubing. However, as the porous plug is disruptive to fluid flow, it may have adversely affected the initial depressurization wave, which would reduce the initial superheat of the liquid methanol when the flash process is initiated and thus reduce the peak cooling.

4.5.3 Effect of initial liquid temperature

The last experimental variable tested, and perhaps the most important one, is the influence of initial liquid temperature on flash cooling rate. From the viewpoint of thermally controlled boiling theory, increases in superheat correspond to higher heat removal rates.

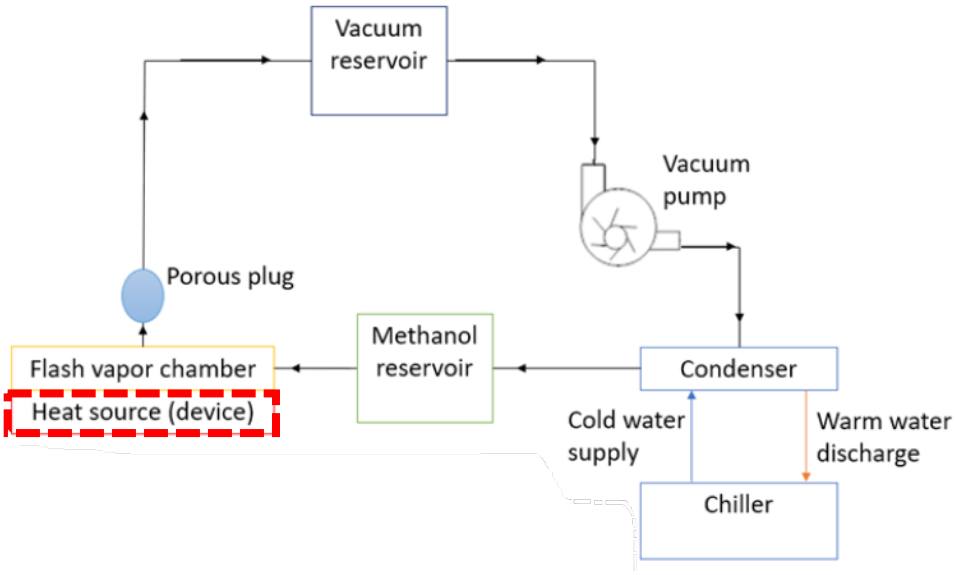

Fig. 4.5.5: Schematic showing relative location of heat source.

It follows that the main approach to maximize heat removal rate would be to increase liquid superheat. To have results comparable to previous experiments that started from steady-state conditions, liquid superheat is directly increased by applying different heat inputs to the filled vapor chamber so different steady-state initial temperatures are attained prior to flash.

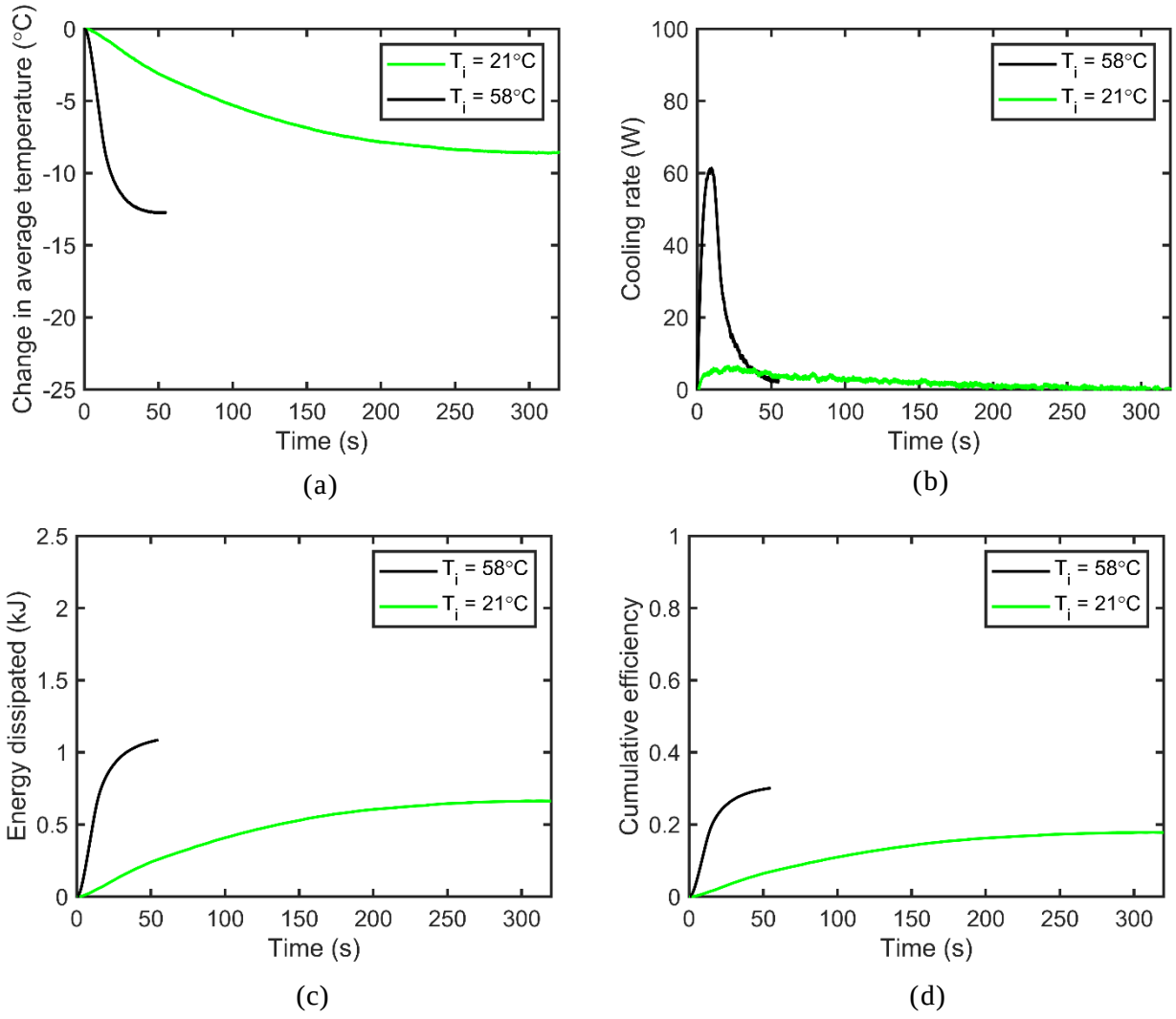

Fig. 4.5.6: Effect of initial liquid temperature for constant vapor chamber filling of 20%. (a) Change in average vapor chamber temperature as a function of time for different initial temperatures. (b) Flash cooling rate, q_{fc}, as a function of time. (c) Cumulative energy dissipation, E_p, as a function of time. (d) Cumulative efficiency, η, as a function of time.

For experimentation, the effect of no heating (0 W) was compared to that with heating (6.2 W), while a porous outflow plug was inserted into the vapor chamber. Due to the general difficulty and uncertainty associated with filling the vapor chamber with the porous plug, only one experiment was done for the 0 W case.

A salient observation from Fig. 4.5.6(b) is the dramatic rise in peak cooling with pre-heating. For the case with pre-heating, the initial temperature attained an average value of 58°C, whereas for the case without heating, the average initial temperature was 21°C. For reference, the saturation temperature of methanol at 1 atm is 64°C, and it was the goal of the heated case of 6.2 W to have the liquid methanol be as close to saturation as possible to maximize the initial superheat. The results shown in Fig. 4.5.6 give evidence for higher flash efficacy with increased heat load.

These results support the notion that increased heat load induces more rapid phase-change, as heat must be absorbed for vaporization to occur. Also, an increase in initial temperature due to increased heat load corresponds to a larger superheat after depressurization. From the viewpoint of thermally controlled boiling theory, increases in superheat correspond to higher heat removal rates. In this regard, to maximize superheat, high initial temperatures and low accumulator pressures are desirable parameters when using flash to maximize peak transient cooling.

4.6 Approach to quantify flash vapor chamber cooling under step heat loads

One application of transient cooling also of high interest is flash cooling efficacy under dynamic heating loads. Fig. 4.5.1(a) showed the sub-ambient cooling of the vapor chamber under constant heating conditions, but in this section, the effect of step heat loads is investigated for constant vapor chamber filling of 20%. Recall from section 4.2 that step heat loads refer to step-changes in heat load applied simultaneously with flash initiation. For these experiments, the

vapor chamber setup was modified to incorporate higher heat fluxes using a resistive heater. Previous results shown in Fig. 4.5.6 demonstrate the importance of initial steady-state conditions prior to flash on maximum cooling rate, and so, for experiments with step heating loads, similar initial temperature conditions are prescribed prior to flash.

Here, the cooling rate due to flash for these sets of experiments is calculated by taking the difference between the thermal response of the vapor chamber with 20% filling under (a) step heating only with no flash and (b) flash with heating. Mathematically, this cooling rate is expressed as:

$$q_{fc}(t) = m_{vapor\ chamber} C_{copper} \left[\frac{dT_{w/o\ flash}(t)}{dt} - \frac{dT_{w/\ flash}(t)}{dt} \right] \tag{11}$$

where $T_{w/o\ flash}(t)$ corresponds to the thermal response of the vapor chamber under step heating with no flash and $T_{w/\ flash}(t)$ corresponds to the thermal response of the vapor chamber undergoing both flash and step heating.

4.7 Results and discussion for flash vapor chamber cooling under step heat loads

The results for flash cooling of the vapor chamber under a step heat load is summarized in the following three sections that report the effects of the magnitude of the applied step heat load, the vapor chamber filling ratio, and dissolved gas in the methanol.

4.7.1 Effect of magnitude of step heat load

$T_{w/o\ flash}(t)$ and $T_{w/\ flash}(t)$ data are shown in Fig. 4.7.1, and corresponding flash cooling as calculated from Eqn. 11 are shown in Fig. 4.7.2.

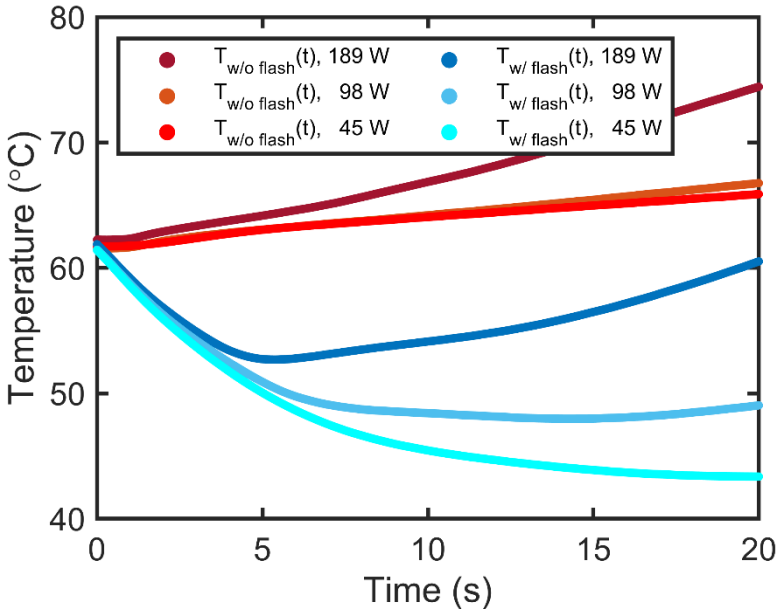

Fig. 4.7.1: Vapor chamber thermal responses to (1) step heating and (2) flash with step heating for constant filling of 20%.

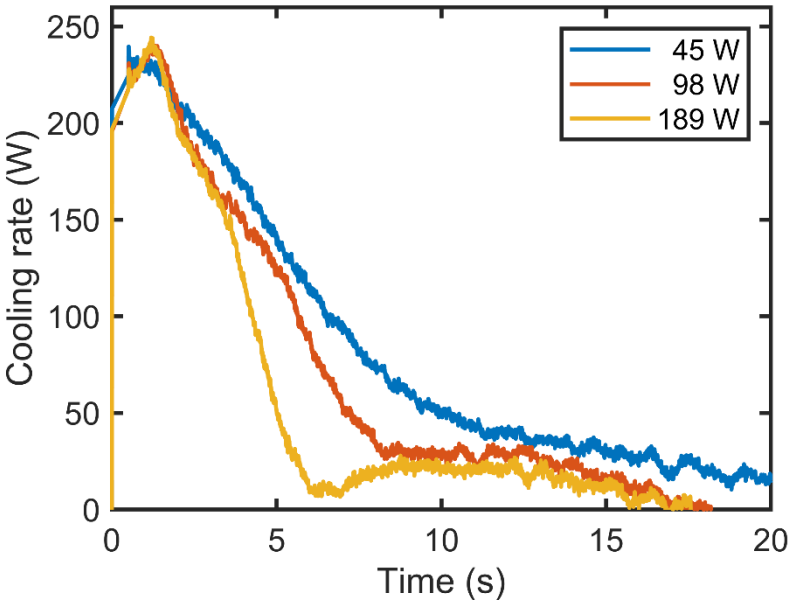

Fig. 4.7.2: Effect of various step heat inputs on flash cooling rate, q_{fc}, for constant 20% vapor chamber filling.

In Fig. 4.7.2, significant transient cooling is achieved with flash, reaching peak cooling above 200 W for all cases within 1.5 s. Compared to Fig. 4.5.1(b), the cooling rate is 3x more than that without step heating, demonstrating the importance of heat input on boiling phenomena even as heat input is timed simultaneously with flash initiation and no anticipatory cooling is present. Additionally, peak cooling seems to be insensitive to heat input, as the filtered data attain similar maximum values, suggesting boiling limits in the vapor chamber have been reached.

Energy dissipated due to flash cooling is considered as follows. Up until 2 s, the flash cooling rates are the same for all applied step heat loads. Thereafter, the flash cooling case corresponding to the lowest applied step heating had the highest total energy dissipation in the vapor chamber, i.e., the vapor chamber was able to stay colder for longer, as shown in Fig. 4.7.1.

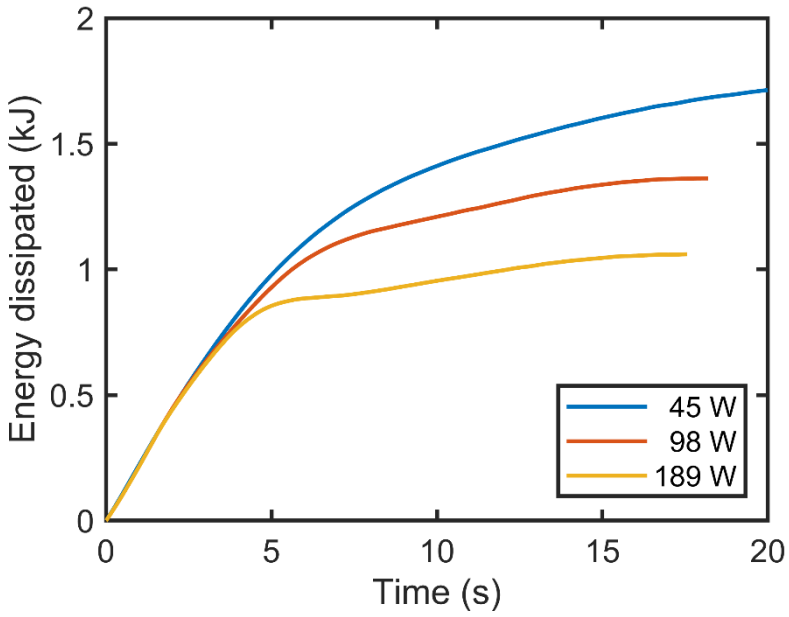

Fig. 4.7.3: Effect of various step heat inputs on flash cooling energy dissipation, E_p, for constant 20% vapor chamber filling.

Comparing the energy dissipated to the maximum theoretical yields Fig. 4.7.4 for flash efficiency. Compared to Fig. 4.5.1(d), the cumulative efficiencies for flash cooling cases with step

heating are higher 20 s after flash initiation, but the final cumulative efficiencies at the end of flash are slightly lower. This reduction in final cumulative efficiency could be due to more pronounced liquid discharge out of the vapor chamber during flash as compared to the prior flash cases under constant heating.

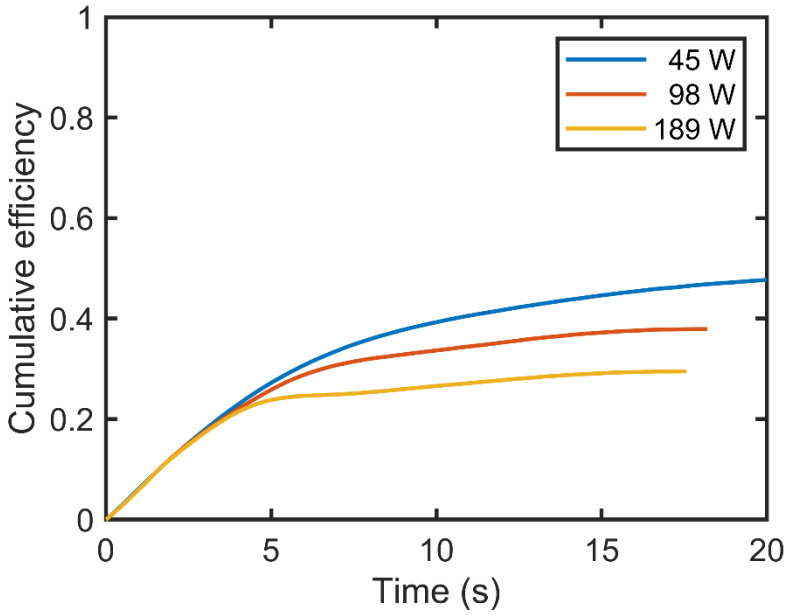

Fig. 4.7.4: Effect of various step heat inputs on flash cooling efficiency, η, for constant 20% vapor chamber filling.

4.7.2 Effect of filling ratio

Next, the effect of various filling ratios on flash vapor chamber cooling for step heating is investigated. The raw data for dynamic heating with varying filling ratios is shown in Fig. 4.7.5.

Using the measured thermal response as shown in Fig. 4.7.5 and Eqn. (11), calculated flash cooling data are shown in Fig 4.7.6. As with the case of flash cooling with step heat load in which magnitude of the heat load was varied, the flash cooling rate reaches over 100 W within 0.005 s. However, one difference is that the initial cooling rate immediately after flash initiation is much more sensitive to filling ratio. While the peak cooling seems to be less sensitive to filling ratio, the

effect of filling ratio on the transient cooling prior to peak cooling may find importance in flash cooling applications that require impulsive cooling responsiveness within sub-second timescales.

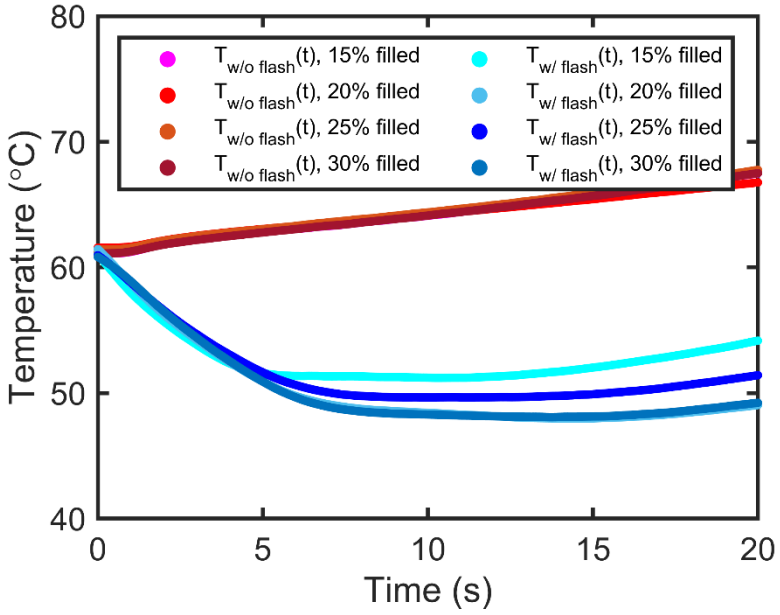

Fig. 4.7.5: Vapor chamber thermal responses to (1) 98 W step heating and (2) flash with 98 W step heating for various filling ratios.

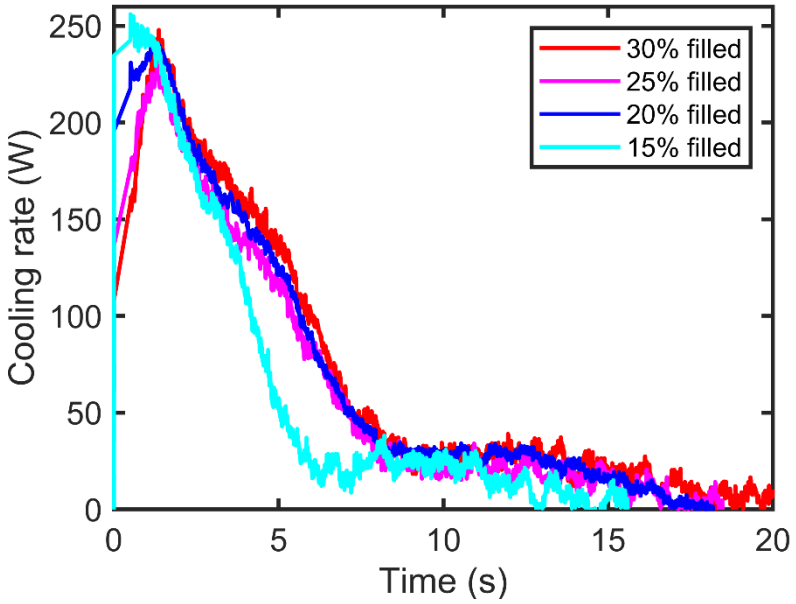

Fig. 4.7.6: Effect of various filling ratios on flash cooling rate, q_{fc}, for constant 98 W step heat input.

Energy dissipated due to flash cooling is shown as follows. The overall trend in energy dissipated is expected, as higher filling ratios are able to supply more cooling due to more available methanol to vaporize and absorb heat. Comparing the energy dissipated to the maximum theoretical yields the following graph for flash efficiency.

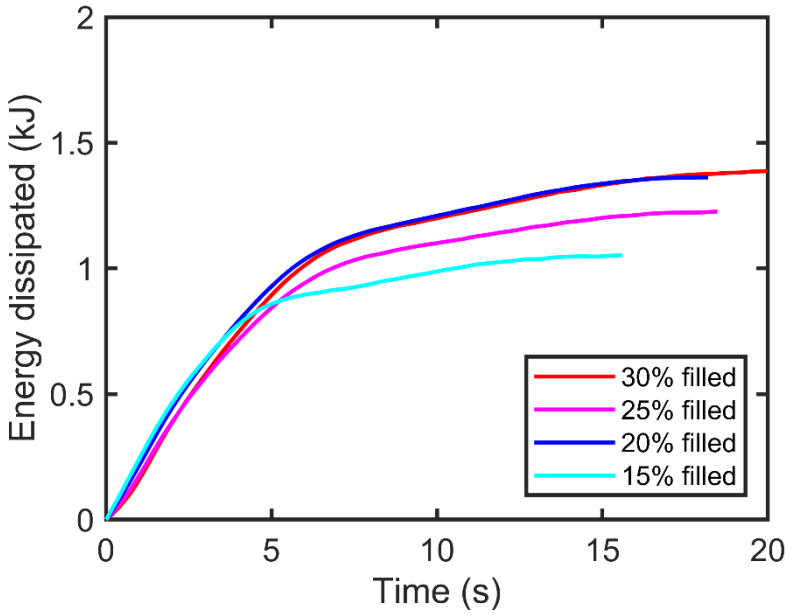

Fig. 4.7.7: Effect of various filling ratios on flash cooling energy dissipation, E_p, for constant 98 W step heat input.

From Fig. 4.7.8, cumulative efficiency is inversely proportional to filling ratio. Lower filling ratios absorb heat more efficiently, and this quality can be attributed to the decreased rate of pressure recovery in the vapor chamber, as show in Fig. 4.3.1, which would allow for more favorable local thermodynamic conditions for boiling.

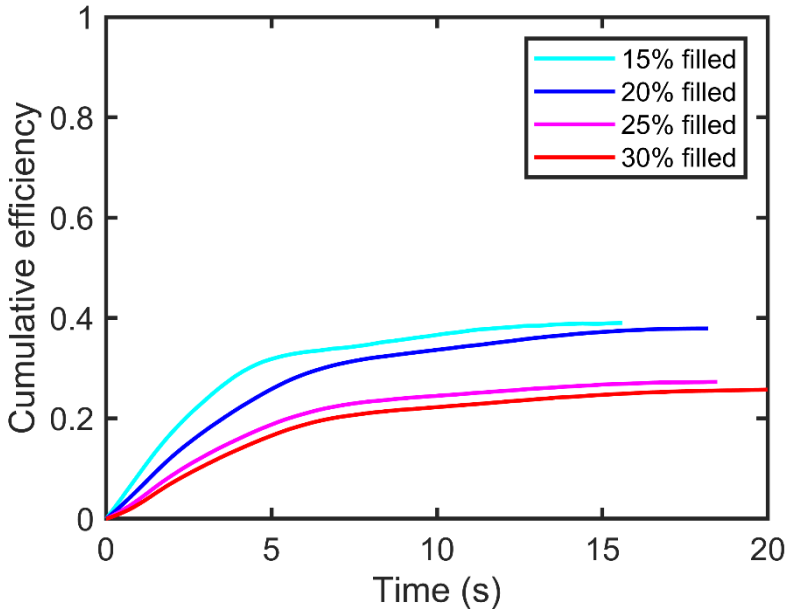

Fig. 4.7.8: Effect of various filling ratios on flash cooling efficiency, η, for constant 98 W step heat input.

4.7.3 Effect of dissolved gas

Another consideration studied in this work is the presence of dissolved gas in the methanol prior to flash. Raw heating data for both aerated and degassed cases are assumed to be equivalent to the case for 98 W step heating as shown in Fig. 4.7.4. For these experiments, the filling ratio was kept constant at 20%. While the original goal was to test degassed methanol at 98 W heating, replacement of the heater used in the experiment (due to malfunction) led to a slight change in heating levels for the same settings on the input power supply.

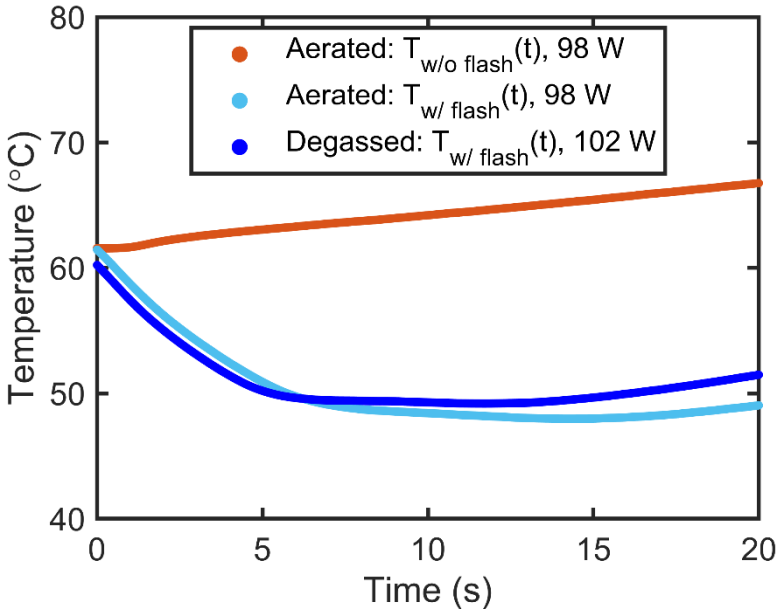

Fig. 4.7.9: Vapor chamber thermal responses to (1) step heating and (2) flash with step heating to investigate role of dissolved gas for nearly constant 100 W step heating.

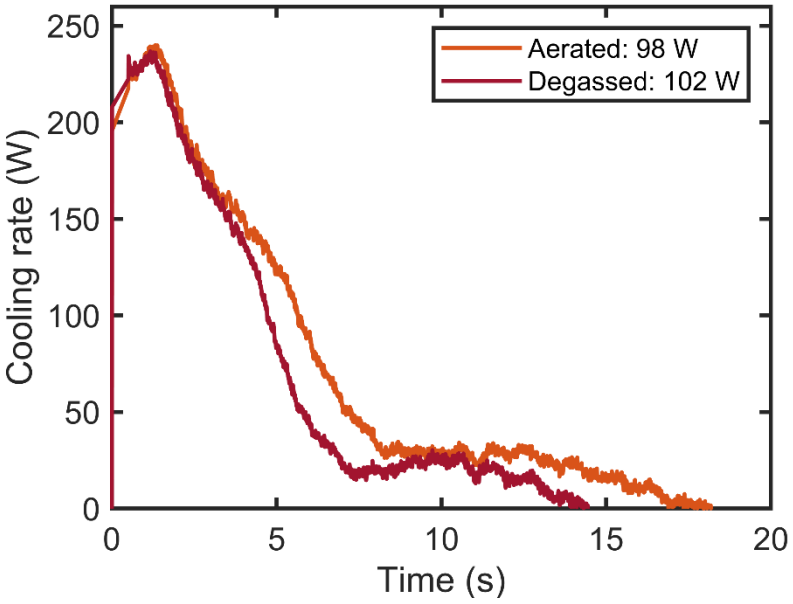

Fig. 4.7.10: Effect of degassing on flash vapor chamber cooling rate, q_{fc}, with constant filling ratio of 20%.

Here, presence of dissolved gas is shown to be mildly helpful for increasing flash cooling rate. Recalling that previous work by Müller-Steinhagen et al. [2.4.1] found that dissolved gas reduces boiling inception superheat, a reasonable postulation is that aerated methanol would be easier to boil due to increases in nucleation sites, and thus would give a higher flash cooling rate than that of degassed methanol. Experimental results as shown in Fig. 4.7.10 indicate that flash cooling rate is higher for aerated methanol, but only for post-peak cooling- the maximum cooling seems to be insensitive to the effects of dissolved gas.

Energy dissipated due to flash cooling is shown in Fig 4.7.11. The effect of dissolved gas is most noticeable after 5 s, in which case flash cooling with aerated methanol can provide more prolonged cooling than degassed methanol. The duration of flash cooling with aerated methanol is 18 s, compared to 14 s for degassed methanol.

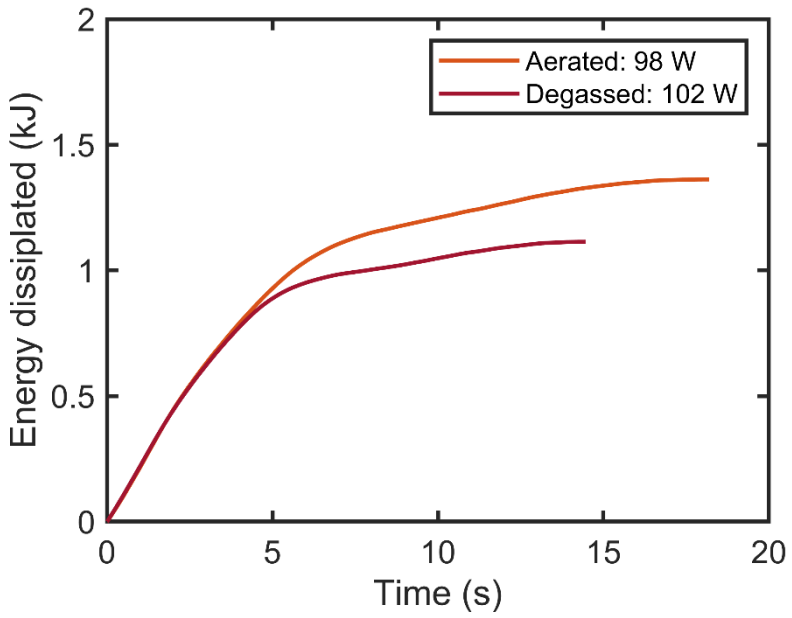

Fig. 4.7.11: Effect of degassing on flash vapor chamber energy dissipation, E_p, with constant filling ratio of 20%.

Comparing the energy dissipated to the maximum theoretical yields the graph in Fig. 4.7.12 for flash efficiency. Comparing these results with the cumulative efficiencies of flash with various filling ratios and step heat loads suggest that the efficiency of the flashing process in the vapor chamber is difficult to improve. Geometric parameters that were not explored, but may affect flash efficacy include diameter of outflow tube and size of vapor chamber.

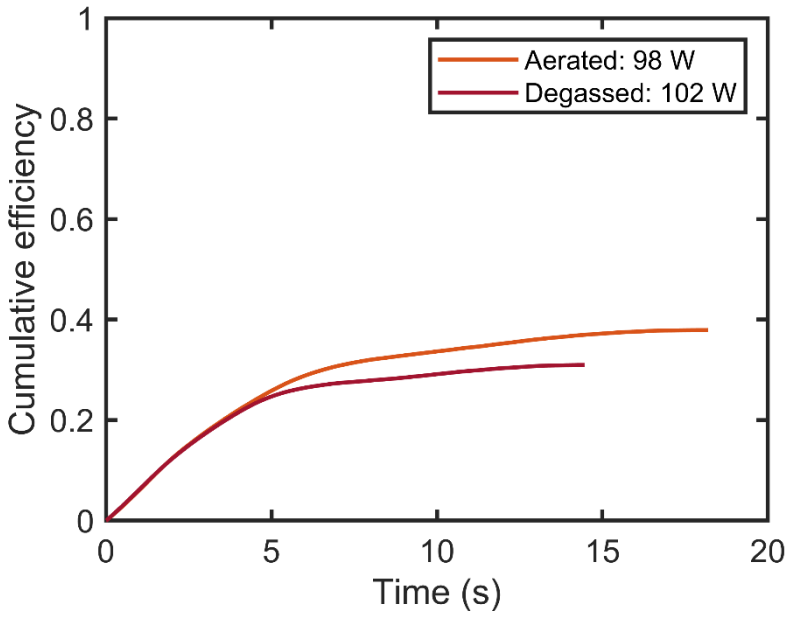

Fig. 4.7.12: Effect of degassing on flash cooling efficiency, η, with constant filling ratio of 20%.

4.8 Regression metrics to quantify flash vapor chamber cooling efficacy

Because flash cooling is inherently a transient phenomenon, a metric capable of capturing change with time is needed. As such, a dual exponential model is implemented [4.8.1] that uses two distinct time constants (and two other fitting parameters) to curve-fit flash cooling data, allowing for quantification of flash cooling rate for both the initial, rapid peak-cooling and the subsequent waning of cooling rate. The general curve-fitting equation is:

$$q_{fc,fitted} = \alpha \frac{\tau_1 \tau_2}{\tau_1 - \tau_2} \left(e^{-\frac{t-\beta}{\tau_1}} - e^{-\frac{t-\beta}{\tau_2}} \right) \quad (12)$$

where $q_{fc,fitted}$ is the fitted flash cooling rate, α and β are fitting parameters, $\tau_1$and τ_2 are time constants (also fitting parameters), and t is time. This functional form has the property of allowing τ_1 and τ_2 to be fully interchangeable. The curve-fitting is applied to cases of constant heating, for cases in which porous plug was either present or absent, as previously shown in Fig. 4.5.1(b) and Fig. 4.5.4, and for cases of different initial temperatures, previously shown in Fig. 4.5.6. In the subsequent sections, regression values obtained for the aforementioned cases are presented and discussed.

4.8.1 Metrics for various filling ratio configurations under a constant heat load

Using the flash vapor chamber cooling experiments conducted with constant heating shown in Fig. 4.5.1 for the implementation of the curve-fitting, good agreement is established between the curve-fitting and the experimental data for the case in which the porous plug is absent. In constructing the curve-fits for Fig. 4.8.1(a), four fitting parameters were used, namely $\alpha, \beta, \tau_1, \tau_2$. However, a constraint can be imposed for β such that $\beta = 0$ s. Physically, this simplification means that the cooling effect due to flash boiling starts instantaneously, which can be considered true because flash initiation, in which the vapor chamber is suddenly depressurized, can be prescribed to begin at $t = 0$ s. Thus, by imposing $\beta = 0$ s to more realistically capture the physical process of flash cooling, the corresponding curve-fit is shown in Fig. 4.8.1(b).

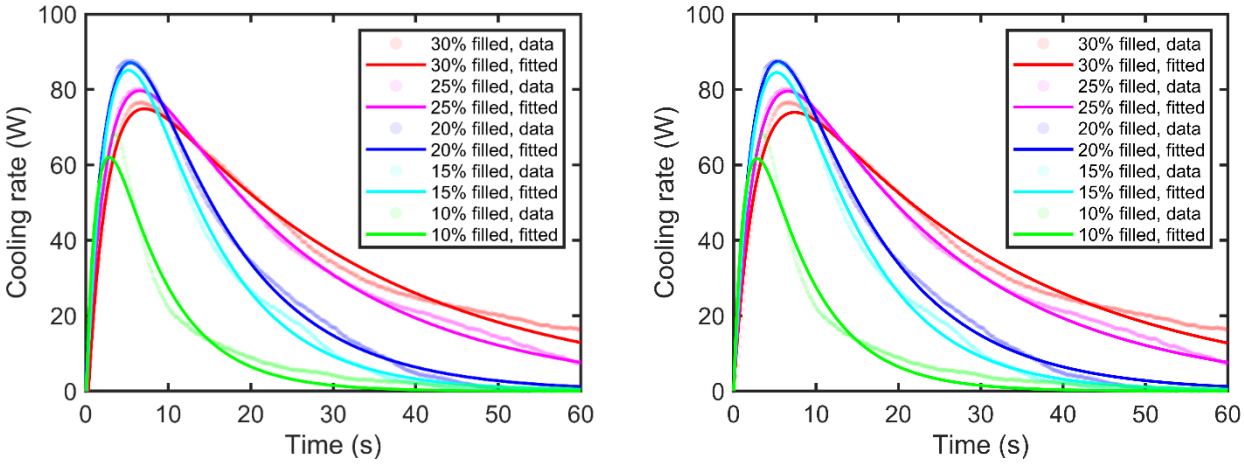

(a) (b)

Fig. 4.8.1: Comparison of data and curve-fitting for flash cooling rate, q_{fc}, under constant 6.2 W heat input and various filling ratios. (a) unconstrained curve-fits. (b) constrained curve-fits, $\beta = 0\ s$.

The fitting parameters α, β, τ_1, and τ_2 associated with the curve-fits are tabulated below. As a guide for interpreting the values, small values of β indicate that flash cooling occurs quickly after rapid depressurization. The larger the value of τ_1, the longer it takes the cooling to wane, and the larger the value of τ_2, the less pronounced the rate of initial cooling is. A scatterplot of τ_1 and τ_2 as functions of vapor chamber filling can be found in Fig. 4.8.3. A scatterplot of α as a function of vapor chamber filling can be found in Fig. 4.8.4.

Table 4.8.1: Fitting parameters associated with flash cooling of vapor chamber under steady 6.2 W heating and various initial amounts of methanol.

Vapor chamber filling (%)	Unconstrained curve-fitting				Constrained curve-fitting			
	α (W)	β (s)	τ_1 (s)	τ_2 (s)	α (W)	β (s)	τ_1 (s)	τ_2 (s)
10	66.46	0.05	6.91	1.40	64.55	0.00	6.89	1.45
15	47.97	0.10	9.57	3.02	46.05	0.00	9.40	3.20
20	46.62	-0.06	11.92	2.96	47.83	0.00	12.02	2.86
25	38.67	0.03	21.53	2.79	38.23	0.00	21.49	2.83
30	37.09	0.32	28.52	2.56	32.79	0.00	28.16	2.93

4.8.2 Metrics for porous plug configurations under a constant heat load

The curve-fitting analysis is also extended to cover the effect of a porous plug at the vapor chamber outlet.

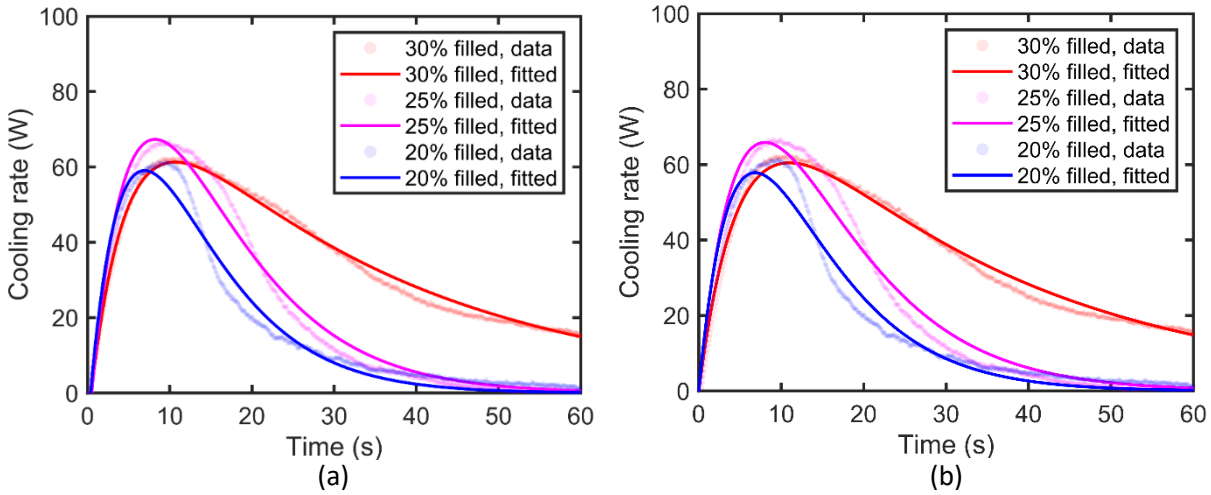

Fig. 4.8.2: Comparison of data and curve-fitting for flash cooling rate, q_{fc}, under constant 6.2 W heat input and various filling ratios, with porous plug at vapor chamber outlet. (a) unconstrained curve-fits. (b) constrained curve-fits, $\beta = 0$ s.

The flash cooling rate curves for the cases with a porous plug are flatter than those without a porous plug, but the curve-fitting still captures the initial rise and decay of the cooling rate well. Corresponding values for the fitting parameters α, β, τ_1, and τ_2 are tabulated and plotted as follows.

Table 4.8.2: Fitting parameters associated with flash cooling of vapor chamber, with porous plug at outlet, under steady 6.2 W heating and various initial amounts of methanol.

Vapor chamber filling (%)	Unconstrained curve-fitting				Constrained curve-fitting			
	α (W)	β (s)	τ_1 (s)	τ_2 (s)	α (W)	β (s)	τ_1 (s)	τ_2 (s)
20	24.51	0.38	6.04	7.14	22.99	0.00	6.84	6.84
25	23.76	0.52	7.71	7.70	22.30	0.00	8.03	8.03
30	18.9	0.47	31.54	4.48	16.96	0.00	30.9	5.09

The small values of β in the unconstrained curve-fitting give strong support for using the physical simplification presented in the constrained curve-fitting. A clearer picture of how τ_1 and τ_2 are influenced by vapor chamber filling is shown as follows in Fig. 4.8.3, for cases with and without the porous plug.

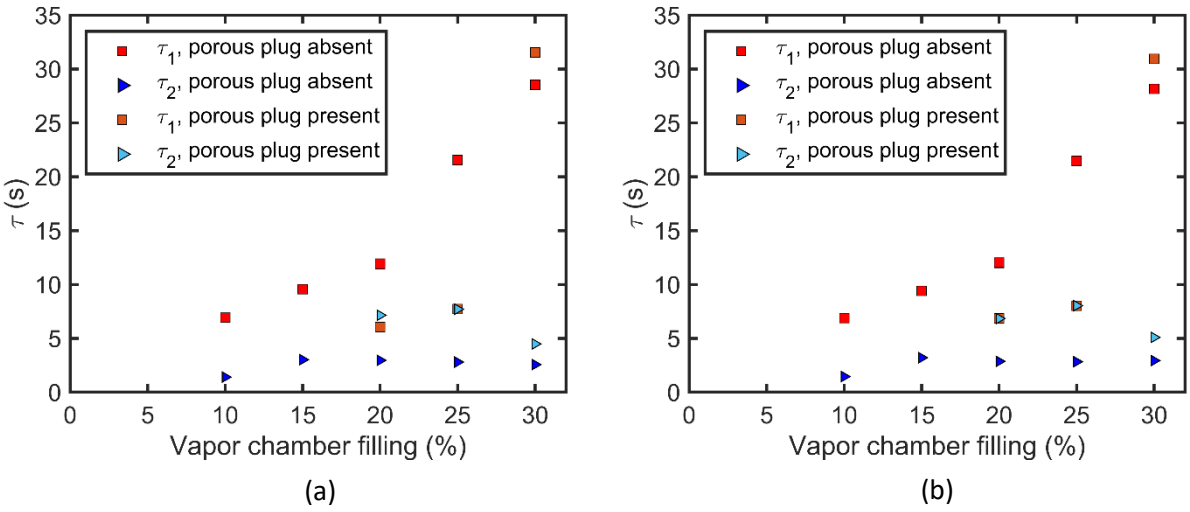

Fig. 4.8.3: Scatterplot of τ_1 and τ_2 as functions of vapor chamber filling for constant 6.2 W heating. (a) unconstrained curve-fitting. (b) constrained curve-fitting, $\beta = 0\ s$.

As the difference between the unconstrained and corresponding constrained curve-fitting parameters are small, only the unconstrained parameters are plotted for α in Fig. 4.8.4. From Fig. 4.8.4, an inverse relationship between α and vapor chamber filling is seen, suggesting that in a general sense (and definitely for above-optimal filling ratios), impact of increased methanol is detrimental to cooling rates attained from flash boiling. From Fig. 4.8.3, some important attributes pertaining to flash cooling and the effect of a porous plug are made clear. First, τ_1 increases with vapor chamber filling, showing how additional methanol present in the vapor chamber contributes to available cooling that persists after peak cooling has been reached. Physically, this explanation is reasonable, as increases in working fluid volume allow for greater

latent heat extraction. Second, the values of τ_2 are relatively small and consistent compared to those of τ_1. Small τ_2 values indicate that the flash process is rapid, as peak cooling is reached quickly. Nearly constant values of τ_2 suggest initial transient cooling is mostly dependent on the thermal mass of the vapor chamber, which was constant for all experiments. Additionally, τ_2 values corresponding to the cases of flash cooling with a porous plug are higher than those without a porous plug, indicating longer duration until peak cooling. This observation is corroborated by noting that for the flash cases without a porous plug, peak cooling is achieved within 10 s (Fig. 4.8.1), but cases with a porous plug, on average, reach peak cooling beyond 10 s of flash initiation.

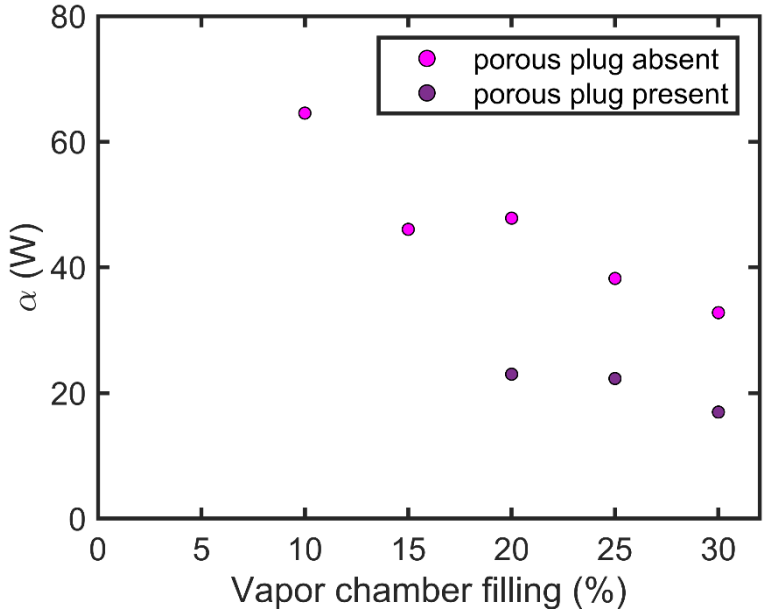

Fig. 4.8.4: Scatterplot of curve-fitting parameter α as a function of vapor chamber filling for constant 6.2 W heating.

4.8.3 Metrics for various initial temperature configurations under constant heat loads

Curve-fitting analysis is also implemented for flash cooling with various initial temperatures. Recall that the curve-fitting is applied to experimental cases in which a constant heat load is applied, and so variation in initial temperature is attributed to variation in applied

heat load. Here, we consider initial temperatures of 58°C and 21°C in which a porous plug is present at the outlet of the vapor chamber. Additionally, we use the constrained curve-fitting approach for which $\beta = 0$ s. For the case with an initial temperature 58°C, a 6.2 W heat load was applied. The corresponding curve-fit was shown previously as the blue curve in Fig. 4.8.2(b), but is reproduced in Fig. 4.8.5(b) as follows.

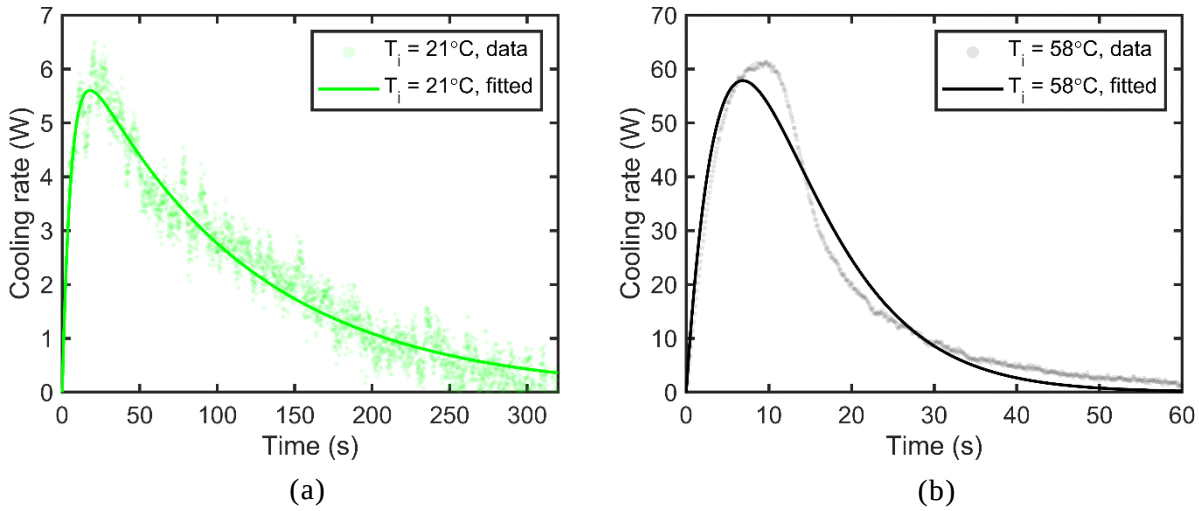

(a) (b)

Fig. 4.8.5: Comparison of data and curve-fitting for flash vapor chamber cooling, q_{fc}, for constant 20% filling ratio and various initial temperatures, with porous plug at vapor chamber outlet. (a) Initial temperature of 21°C. (b) Initial temperature of 58°C.

Table 4.8.3: Fitting parameters associated with flash cooling of vapor chamber, with porous plug at outlet, under constant 20% filling ratio and various initial temperatures.

Initial temperature (°C)	Constrained curve-fitting			
	α (W)	β (s)	τ_1 (s)	τ_2 (s)
21	1.14	0.00	107.50	5.83
58	22.99	0.00	6.84	6.84

Values for the fitting parameters α, β, τ_1, and τ_2 are shown in Table 4.8.3. While differences in flash cooling due to variation in initial temperature are significant, the results for

the curve-fitting time constants show similarity in values of τ_2. For this case of variable initial temperature, τ_2 attains an average value of 6.33. Compared to other experiments with a porous plug for cases of variable filling ratios, from Table 4.8.2, τ_2 attains an average value of 6.65. Thus, it is observed that τ_2 seems to be independent of loading condition, and only on the geometric factors concerning the vapor chamber. For example, when the porous plug is absent, τ_2 attains an average value of 2.65.

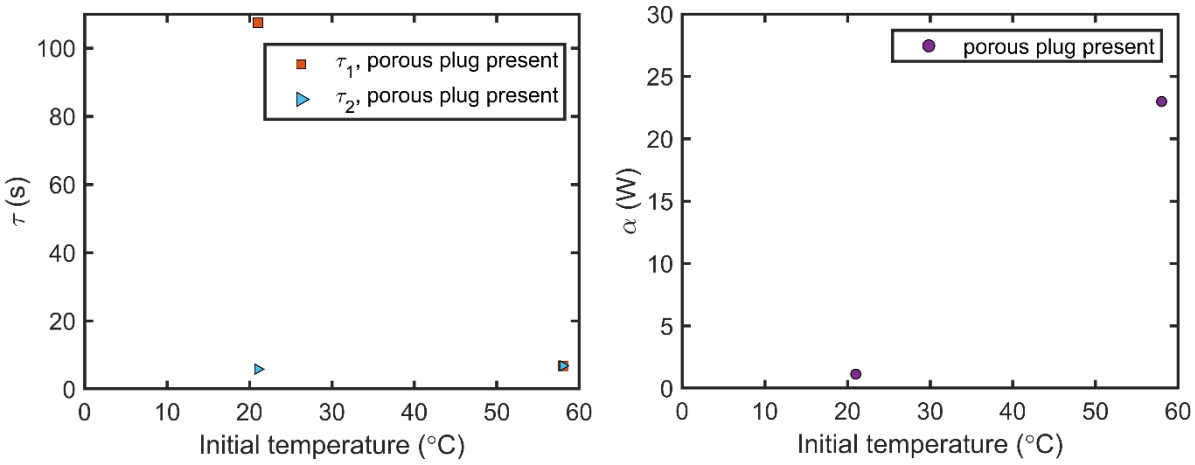

(a) (b)

Fig. 4.8.6: *Scatterplot of curve-fitting parameters as functions of initial temperature for constant 20% filling ratio. (a)* τ_1 and τ_2. (b) α.

4.8.4 Metrics for various magnitude of step heat load configurations

Regression up to this section was applied for flash cooling cases in which constant heating was applied before and maintained after flash initiation. However, transient cooling is also useful for systems that undergo dynamic heat loads. To address the efficacy of curve-fitting for step heat loads, the same constrained curve-fitting approach is applied to flash cooling with step heating for cases of variable magnitudes of step heat loads and variable filling ratios, as was shown in sections 4.7.1 and 4.7.2, respectively. As a reminder, all experiments regarding the flash vapor chamber under various step heat loads and variable filling ratios were conducted without the use of a porous plug and started at initial temperatures around 61°C and initial pressures of 101 kPa.

The curve-fits for flash cooling at 45 W, 98 W, and 189 W step heat loads are shown in Fig. 4.8.7, with corresponding data taken previously shown in Fig. 4.7.2. Due to the high initial rate of increase in cooling rate, curve-fitting overestimates peak cooling, but generally captures the subsequent waning of cooling rate. However, for high heat transient loads, especially 189 W, there is a local minimum in measured cooling rate at 6.5 s that is not captured by the curve-fitting model.

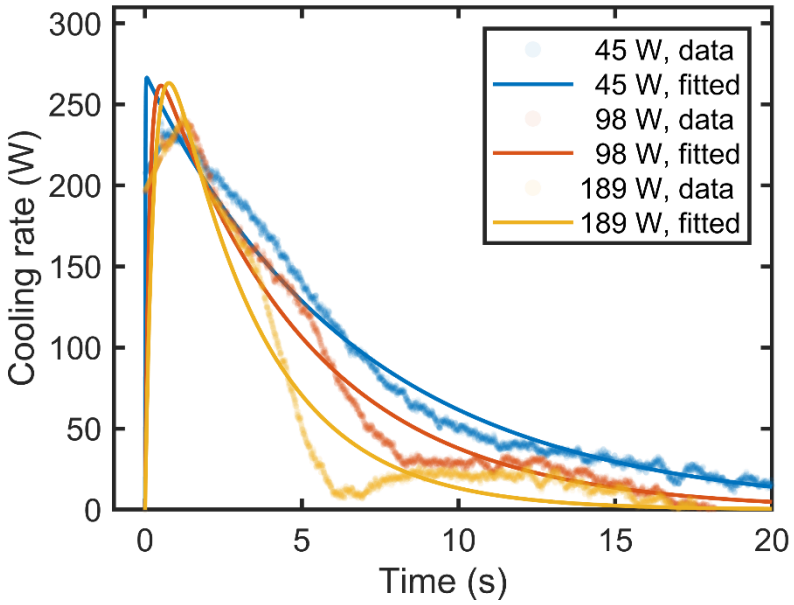

Fig. 4.8.7: Comparison of data and curve-fits for flash vapor chamber cooling, q_{fc}, under various step heat loads and constant 20% filling ratio.

Corresponding parameters associated with flash cooling under these step heating conditions are shown in Table 4.8.4 and plotted in Fig. 4.8.8. In plotting the fitting parameters as functions of step heat load, a few observations are made concerning the evolution of τ_1 and τ_2 with heat load. The inverse proportionality between τ_1 and heat load indicates that higher heat load results in faster decay of flash cooling. This relationship is expected since, for a constant filling ratio, total energy available for flash cooling is conserved, i.e., flash cooling can either offset a high

heat load for a short duration or a lower heat load for a longer duration. On the other hand, τ_2 varies directly with heat load. This relationship indicates that high step heat loads result in lower initial rates of cooling, which can be explained by the decreased depressurization rates associated with high step heat loads as shown in Fig. 4.3.4. Decreased depressurization rate is due to rapid vapor generation following flash boiling, which is aided by increases in heat load, as boiling is an energy-intensive process.

Table 4.8.4: Fitting parameters associated with flash vapor chamber cooling under various step heat loads and constant 20% filling ratio.

Step heat load (W)	Constrained curve-fitting			
	α (W)	β (s)	τ_1 (s)	τ_2 (s)
45	32470	0.00	6.78	0.01
98	2097	0.00	4.83	0.14
189	1145	0.00	2.99	0.30

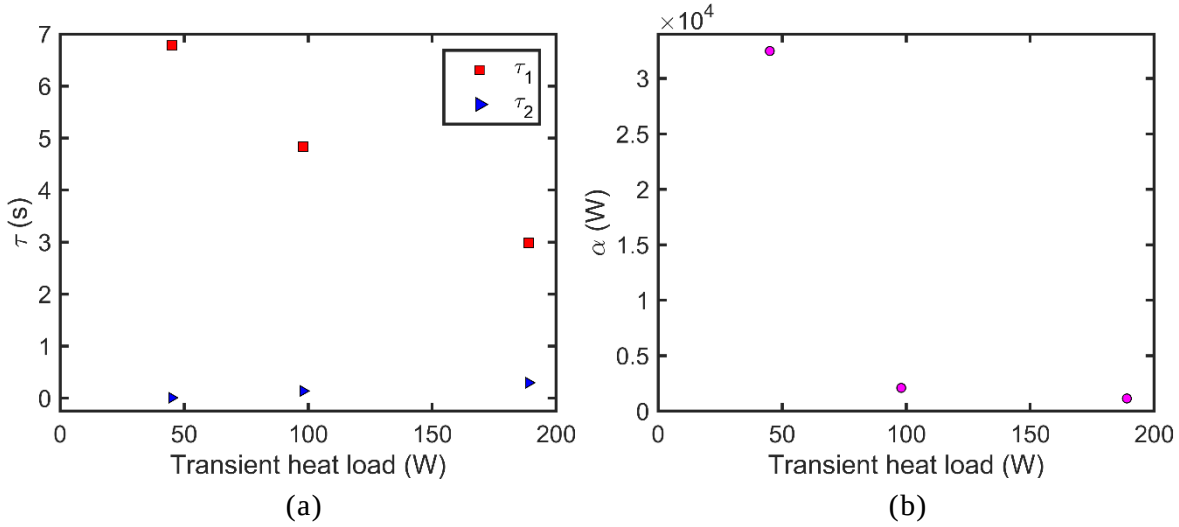

Fig. 4.8.8: Curve-fitting parameters as functions of step heat load for flash vapor chamber cooling under various step heat loads and constant 20% filling ratio. (a) τ_1 and τ_2. (b) α.

4.8.5 Metrics for various filling ratio configurations under a step heat load

The final regression analysis concerns flash cooling with step heating for cases of variable filling ratios from 15% to 30%. Corresponding curve-fits with experimental flash cooling data are plotted in Fig. 4.8.9. As for the case of flash cooling under various step heat loads from Fig. 4.8.7, curve-fitting overestimates peak cooling due to the high initial rates of increase in cooling rate. However, this aspect diminishes with increasing filling ratio since the sharpness of the initial transients reduces with increasing filling ratio.

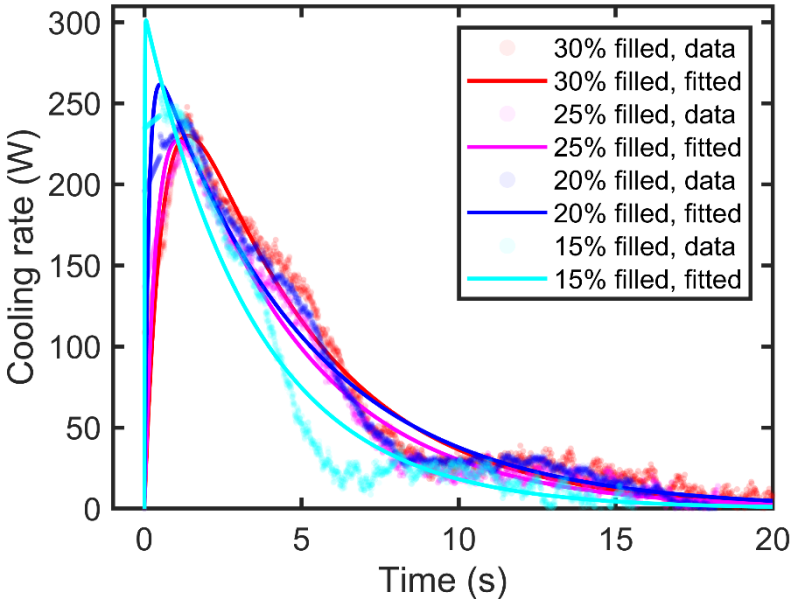

Fig. 4.8.9: *Comparison of data and curve-fits for flash vapor chamber cooling, q_{fc}, under a 98 W step heat load and various filling ratios.*

Parameters corresponding to the regression analysis are tabulated in Table 4.8.5 and plotted in Fig. 4.8.10. A few observations are noted. The sharpness of the initial transients, shown by values of τ_2, varies directly with vapor chamber filling, indicating that liquid methanol in the vapor chamber with low filling ratios more readily vaporizes under a specified step heat load than that of higher filling ratios. This observation is in direct contrast to Fig. 4.8.3(b), in which τ_2

remains constant for various filling ratios while τ_1 varies significantly with filling ratio. To summarize, filling ratio affects flash cooling differently depending on the loading condition: for flash cooling under constant heating, filling ratio most prominently affects the wane of flash cooling past peak cooling, and for flash cooling under step heating, filling ratio affects the initial rise of flash cooling up to peak cooling. Aside from the time constants, Fig. 4.8.4 (for the porous plug absent case) and Fig. 4.8.10(b) both indicate an inverse relationship between α and filling ratio, but is more pronounced for the case in which step heating is applied.

Table 4.8.5: Fitting parameters associated with flash vapor chamber cooling under a 98 W step heat load and various filling ratios.

Vapor chamber filling (%)	Constrained curve-fitting			
	α (W)	β (s)	τ_1 (s)	τ_2 (s)
15	35280	0.00	3.54	0.01
20	2098	0.00	4.83	0.14
25	703	0.00	4.20	0.42
30	519	0.00	4.31	0.61

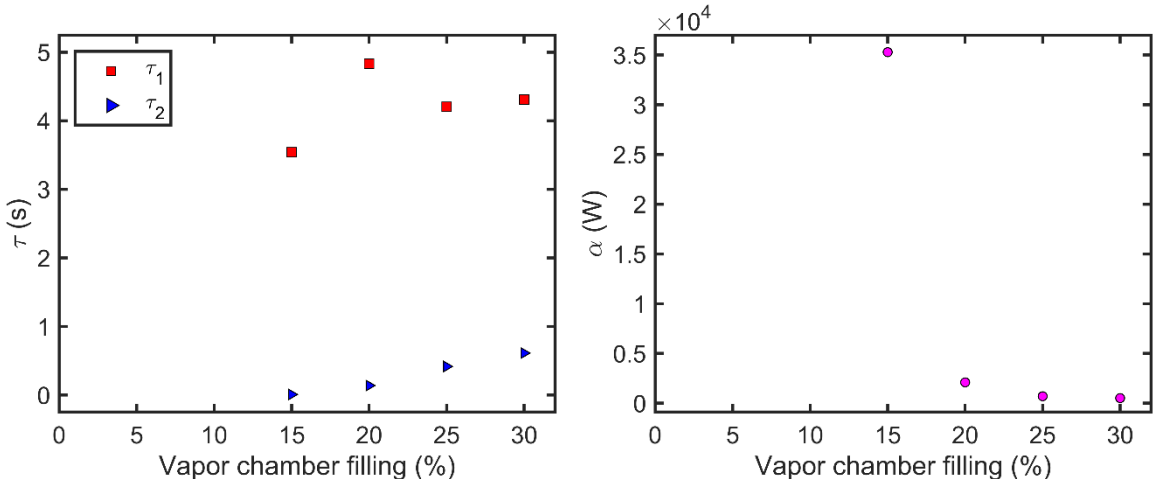

(a) (b)

Fig. 4.8.10: *Curve-fitting parameters as functions of vapor chamber filling for flash vapor chamber cooling under 98 W step heat loads and various filling ratios. (a)* τ_1 and τ_2. (b) α.

Thus, with extraction of curve fitting parameters and two time constants associated with flash, general qualities of time to peak cooling and rate of decay of cooling can be quantified and compared between not only various flash cooling trials, but other transient cooling solutions as well. Additionally, as α, β, τ_1, and τ_2 are plotted as functions of filling ratio and initial temperature, flash cooling rate can be predicted using Eqn. (12) for different vapor chamber configurations. This regression-based approach allows for the design of a cooling system that can be selected to dissipate thermal loads in a transient manner.

Chapter 5: Conclusion

Flash cooling is an approach to transient thermal management in which system pressure is quickly modulated to induce sudden boiling for rapid cooling. As typical cooling solutions operate in steady-state, flash cooling offers dynamic cooling for short heat loads known *a priori*.

For this work, experiments were conducted on a flash vapor chamber assembly to quantify transient cooling rate. Results showed that peak cooling above 200 W when heating is applied simultaneously with flash initiation for vapor chamber filling ratios above 15%. Flash inception, or the onset of vaporization, was investigated with both pressure wave propagation experiments and analysis of the flash vapor chamber data. From the pressure wave propagation experiments, pressure undershoot was shown to be an important factor in determining local vaporization. This setup was used to investigate the fundamental nature of depressurization in a tube. As for flash vapor chamber data, flash onset was shown to begin at an average superheat of roughly 5°C. This value shows that flash boiling is initiated at thermodynamic conditions corresponding to heterogeneous boiling, while retaining the rapidity and bulk vaporization properties of homogeneous boiling.

Flash is promising in its ability to offset transient loads, and the experiments were done for single pulse heat loads. However, real applications may require pulsed cooling or anticipatory cooling. Considering that the low static pressure at high altitudes can be readily exploited for flash cooling, the gamut for potential applicability of flash cooling is wide for both aerospace systems. In this work, basic insights into flash cooling were presented, and while transient thermal management is still an important area of consideration for the thermal engineer, this work presented both metrics in which other transient cooling methods can be compared and a framework in which transient flash cooling over its entire duration can be modeled for various systems parameters such as filling ratio and initial temperature.

Appendix

A.1 Choice of working fluid

The ideal working fluid has the following properties: high latent heat, high thermal conductivity, low liquid and vapor viscosities, low surface tension, and low freezing point. Additionally, the working fluid must be compatible with the tubing in which the fluid is transported, namely copper and polypropylene [A.1.1].

Table A.1: Selection of working fluid.

Working Fluid	Freezing point (°C)	Boiling point (°C)	Latent heat (kJ/kg)	Surface tension (mN/m)	Copper compatibility	Polypropylene compatibility
Ethanol	-112	78	846	22	Excellent	Excellent
Methanol	-98	64	~1000	22	Good	Excellent
Water	0	100	2256	72	Good	Excellent
Acetone	-95	57	518	25	Excellent	Excellent
Pentane	-129	36	~350	16	N/A	Poor
R-134A	-103	-26.3	217	8.5	Excellent	Good
HFE7100	-135	61	125	13.6	Good	Good
Ammonia	-78	-33	1369	23	N/A	Excellent
Dowtherm	12	257	407	40	Good	N/A
Heptane	-91	98	318	20	Excellent	Fair

A.2 Details about pressure wave propagation setup

Regarding the sensors used in the experiment, the experimental setup was constructed so that the pressure wave propagation between the two pressure gauges could be picked up within the gauge sampling rate. The local acoustic speed in methanol is about 1100 m/s, and the distance between PT-in and PT-reflect is 1.5 m, giving a wave travel time of about 1 ms. The sampling rate of the pressure gauge is rated for 1 kHz, and the sampling rate data acquisition system that collects pressure gauge data was also for 1 kHz. By doing this, the pressure wave propagation is accurately captured. Thermocouple responsiveness is a lot slower, on the order of 0.1s, but due to the nature

of the experiments in measuring pressure wave propagation, and not thermophysical properties during flash per se, the sampling rate for the thermocouples was of lesser significance than that of the pressure gauges. However, temperature measurements on the outside of the tube offer insights into overall transport phenomena inside the tube.

Multiple sources of error exist within the experimental system, mainly regarding pressure and vacuum level measurements. One source of pressure measurement error stems from the actual liquid column height of methanol between experimental trials. This was mitigated by using valves to close off the tube exit leading to the vacuum reservoir between experimental trials and having a pressurized methanol reservoir to favor filling the long tube as much as possible during filling. The tube connecting the solenoid valve to the vacuum reservoir is constructed of clear plastic, so it was visible when excess methanol would seep out of the tube after filling. Assuming the variability in liquid height varies between the valve leading to the vacuum reservoir and the clear tube, the variability in pressure measured by the pressure gauges due to changes in hydrostatic head is about 2 kPa. Another source of pressure measurement error was found while running experiments, whereby it was found that a more significant cause of variation in initial pressures before depressurization occurs from the gradual increase in pressure within the tube, presumably due to the increase in partial pressure of the methanol once the tube is sealed from the ambient environment before each depressurization trial. The maximum variability in initial pressures before flash was measured to be 5 kPa, corresponding to a final depressurization to 30 kPa. This final depressurization had the largest variability in initial pressures due to the increase in time required for the vacuum pump to reach 30 kPa, which allowed the pressure in the tube to build up, thus being a source of random error. As for error in prescribing the vacuum level, the final prescribed pressures vary by ± 1 kPa, which correspond to half-tick marks on a manual pressure gauge connected to the vacuum reservoir. The vacuum level was set manually, and so, represents a source of human systematic error.

A.3 Details about flash vapor chamber experimental setup

In addition to the vapor chamber as the desired hardware for measuring flash cooling efficacy (courtesy of Aavid Thermacore), a thermal-fluid test setup was constructed to ensure accurate fluid transport and experimental repeatability. Referring to Fig 4.2.1, important hardware consists of a methanol reservoir and accumulator, (identical 11.4 L stainless steel pressure vessels), a vacuum pump (Edwards RV3), K-type thermocouples (Omega SAI-K), and pressure transducers (Omega PX419-030AI). For experiments with a porous plug, steel wool was compacted and inserted into the single tube connected to the vapor chamber. To make the test setup as leakproof as possible, metal tubing and Swagelok compression fittings were used wherever possible, and all joints were covered with vacuum grease. Also, to minimize effects of temperature fluctuations due to changes in ambient room temperature, melamine foam and insulation tape were wrapped around the vapor chamber.

Data acquisition and experimental control was done through LabVIEW using a micro-controller (NI CompactDAQ). An in-house developed state-machine-based code allows for valve control, monitoring of temperature and pressure data, and start/stop of data collection. The experimental data is formatted as a five-row text document, with the first row corresponding to vacuum reservoir pressure, second row vapor chamber pressure, third row top vapor chamber temperature, and fifth row bottom vapor chamber temperature. The fourth row is unused.

A.4 Readme for MATLAB code used for flash vapor chamber analysis

This section presents an outline of the MATLAB code used to analyze experimental data. The code is divided into various sections- the first section must be run first, and it is advised to run all preceding sections before the desired section due to shared variables used throughout the code. Outputs of each section are summarized below.

Section 1: must run this section first

- No figures, only calculates parameters needed for plotting in subsequent sections

Section 2: flash with step heating, and curve-fitting

- Figure 1: heating vs. time and flash cooling vs. time for various step heat inputs
- Figure 2: q vs. t for various step heat inputs
- Figure 3: q vs. t for various step heat inputs and constant 20% filling ratio, with corresponding constrained curve-fits ($\beta = 0$)
- Figure 4: time constants vs. step heat input for flash with constant 20% filling ratio
- Figure 5: curve fitting parameter α vs. step heat input for flash with constant 20% filling ratio
- Figure 6: energy dissipated vs. t for various step heat inputs
- Figure 7: efficiency vs. t for various step heat inputs
- Figure 8: heating vs. time and flash cooling vs. time for various filling ratios
- Figure 9: q vs. t for various filling ratios
- Figure 10: q vs. t for various filling ratios, 98 W step heating, with corresponding constrained curve-fits ($\beta = 0$)
- Figure 11: time constants vs. filling ratio for flash with 98 W step heating
- Figure 12: curve fitting parameter α vs. filling ratio for flash with 98 W step heating

- Figure 13: energy dissipated vs. t for various filling ratios
- Figure 14: efficiency vs. t for various filling ratios
- Figure 15: heating vs. time and flash cooling vs. time for aerated/degassed methanol
- Figure 16: q vs. t for aerated/degassed methanol
- Figure 17: energy dissipated vs t. for aerated/degassed methanol
- Figure 18: efficiency vs t. for aerated/degassed methanol

Section 3: flash with constant heating, and curve-fitting

- Figure 1: q vs. t for various filling ratios (porous plug absent)
- Figure 2: q vs. t for various filling ratios (porous plug present), and corresponding unconstrained curve-fits
- Figure 3: q vs. t for various filling ratios (porous plug present), and corresponding constrained curve-fits ($\beta = 0$)
- Figure 4: q vs. t for various filling ratios (porous plug absent) and corresponding unconstrained curve-fits
- Figure 5: q vs. t for various filling ratios (porous plug absent) and corresponding constrained curve-fits ($\beta = 0$)
- Figure 6: τ_1 and τ_2 vs. filling ratio (for both porous plug absent and porous plug present) for case of unconstrained curve-fitting
- Figure 7: τ_1 and τ_2 vs. filling ratio (for both porous plug absent and porous plug present) for case of constrained curve-fitting ($\beta = 0$)
- Figure 8: α vs. filling ratio (for both porous plug absent and porous plug present) for case of constrained curve-fitting
- Figure 9: τ_1 and τ_2 vs. filling ratio (for porous plug present) for case of constrained curve-fitting ($\beta = 0$)

- Figure 10: α vs. initial temperature (for porous plug present) for case of constrained curve-fitting

Section 4: flash with constant heating, porous plug focus

- Figure 1: energy dissipated vs. time for various initial temperatures (58°C and 21°C) Optional: energy dissipated vs. time for various filling ratios
- Figure 2: Efficiency vs. time for two cases with porous plug and 20% filling: (1) 58°C and (2) 21°C
- Figure 3: Change in temperature vs. time for two cases with porous plug and 20% filling: (1) 58°C and (2) 21°C
- Figure 4: q vs. t for various initial temperatures (58°C and 21°C)
- Figure 5: constrained curve-fit ($\beta = 0$) for flash at initial temperature of 58°C
- Figure 6: constrained curve-fit ($\beta = 0$) for flash at initial temperature of 21°C

Section 5: flash with step heating, pressure data focus

- Figure 1: vapor chamber pressure vs. time and flash onsets for various step heat inputs
- Figure 2: absolute pressure required for flash, for various step heat loads
- Figure 3: superheat for various step heat loads

Section 6: unused graphs (but still informative)

- Figure 1: vacuum reservoir pressure vs. time for all data
- Figure 2: vapor chamber pressure vs. time, vacuum reservoir pressure vs. time, driving pressure vs. time, and bubble onset for all data
- Figure 3: specific internal energy vs. time
- Figure 4: predicted methanol temperature during flash vs. time

Section 7: P-T diagram for methanol, calculated from CoolProp

- Figure 1: P-T diagram for methanol, with dot for typical initial state

Section 8: testing raw data and goodness of fit for filter used in flash analysis with step heat loads

- Figure 1: raw temperature and filtered temperature vs. time for arbitrary data
- Figure 2: raw vapor chamber pressure and vacuum reservoir pressure vs. time for arbitrary data

References

[1.1.1] J. D. Engerer, “RAPID TRANSIENT COOLING UTILIZING FLASH BOILING AND DESPORTION ON GRAPHITIC FOAMS,” Ph.D. dissertation, School of Mech. Eng., Purdue Univ., West Lafayette, IN, USA, 2016.

[1.1.2] *Degraded Visual Environment*, IMSAR LLC, Accessed on: May 30, 2021. [Online]. Available: https://www.imsar.com/portfolio/degraded-visual-environment/

[1.3.1] *Geothermal Electricity Production Basics*, National Renewable Energy Laboratory. Accessed on: May 20, 2021. [Online]. Available: https://www.nrel.gov/research/re-geo-elec-production.html

[1.3.2] Britannica, The Editors of Encyclopaedia, *Desalination*, Encyclopedia Britannica, September 6, 2019. Accessed on: May 20, 2021. [Online]. Available: https://www.britannica.com/technology/desalination#ref1120970

[1.3.3] *Nuclear 101: How Does a Nuclear Reactor Work?*, Office of Nuclear Energy, March 29, 2021. Accessed on: May 20, 2021. [Online]. Available: https://www.energy.gov/ne/articles/nuclear-101-how-does-nuclear-reactor-work

[1.3.4] *Chernobyl Accident and Its Consequences*, Nuclear Energy Institute, May 2019. Accessed on: May 20, 2021. [Online]. Available: https://www.nei.org/resources/fact-sheets/chernobyl-accident-and-its-consequences

[1.3.5] *Environmental Control and Life Support System*, Proactive Information Corporation, Accessed on: May 20, 2021. [Online]. Available: https://spaceshuttleguide.com/system/environmental%20Controls.htm#FLASH_EVAPORATOR_SYSTEM

[1.3.6] *V-Chiller*, V-Chiller, 2018. Accessed on: May 20, 2021. [Online]. Available: http://www.vchiller.com/

[1.3.7] Rapid cooling apparatus, by D. Reznik. (2000, Dec. 20). Patent 6,158,104 [Online]. Available: https://patents.google.com/patent/US6158504

[1.3.8] D. Reznik, *Rapid Vacuum Cooler*. Accessed on: May 20, 2021. [Online]. Available: http://www.raztek.com/techinfo.html#Cooler

[1.3.9] J. Barták, "A study of the rapid depressurization of hot water and the dynamics of vapour bubble generation in superheated water," *International Journal of Multiphase Flow*, vol. 16, no. 5, pp. 789-798, 1990.

[1.3.10] Y. Hanaoka, K. Maeno, L. Zhao and G. Heymann, "A Study of Liquid Flashing Phenomenon Under Rapid Depressurization," *JSME International Journal, Series 2: Fluids Engineering, Heat Transfer, Power, Combustion, Thermophysical Properties,*, vol. 33, no. 2, 1990.

[1.3.11] Q. Zhang, Q. Bi, J. Wu, J. Liang and W. Wang, "Experimental investigation on the rapid evaporation of high-pressure R113 liquid due to sudden depressurization," *International Journal of Heat and Mass Transfer*, vol. 61, pp. 646-653, 2013.

[1.3.12] D. Saury, S. Harmand and M. Siroux, "Flash evaporation from a water pool: Influence of the liquid height and of the depressurization rate," *International Journal of Thermal Sciences*, vol. 44, no. 10, pp. 953-965, 2005.

[1.3.13] E. Hahne and G. Barthau, "Evaporation waves in flashing processes," *International Journal of Multiphase Flow*, vol. 26, no. 4, pp. 531-547, 2000.

[1.3.14] K. Miyazaki, Y. Fujii-E, and T. Suita, "Propagation of pressure wave in air-water two-phase system, (I)," *Journal of Nuclear Science and Technology*, vol. 8, no. 11, pp. 606-613, 1971.

[1.3.15] W. L. Cheng, Y. H. Peng, H. Chen, L. Hu and H. P. Hu, “Experimental investigation on the heat transfer characteristics of vacuum spray flash evaporation cooling,” *International Journal of Heat and Mass Transfer*, vol. 102, pp. 233-240, 2016.

[1.3.16] L. Hao, “Analysis of bubble growth and motion dynamics in superheated liquid during flash evaporation,” *International Journal of Heat and Mass Transfer*, vol. 151, no. 119356, 2020.

[1.3.17] U. Shah, M. Ma, M.T. Barako, A. Bar-Cohen, S.S. Iyer, T.S. Fisher, “Experimental demonstration of pressure-driven flash boiling for transient two-phase cooling,” *IEEE Transactions on Components and Packaging Technologies*, manuscript accepted for publication, 2021. DOI: 10.1109/TCPMT.2021.3085876

[2.2.1] V.K. Dhir, “Chapter 4 Nucleation and bubble growth”, to be published.

[2.2.2] Y.Y. Hsu, “On the size range of active nucleation cavities on a heating surface,” *Journal of Heat Transfer*, vol. 84, no. 3, pp. 207-213, 1962.

[2.4.1] H. Müller-Steinhagen, N. Epstein, and A.P. Watkinson, “Effect of dissolved gases on subcooled flow boiling heat transfer,” *Chemical Engineering and Processing: Process Intensification*, vol. 23, no 2, pp. 115-124, 1988.

[3.3.1] S.S. Chen and M.W. Wambsganss, “Design guide for calculating natural frequencies of straight and curved beams on multiple supports,” Argonne National Laboratory, Argonne, IL, USA, Tech. Rep. ANL-CT-74-06, June 1974.

[4.4.1] I. H. Bell, J. Wronski, S. Quoilin, and V. Lemort, "Pure and Pseudo-pure Fluid Thermophysical Property Evaluation and the Open-Source Thermophysical Property Library CoolProp," Industrial & Engineering Chemistry Research, vol. 53, no. 6, pp. 2498-2508, 2014.

[4.5.1] J. D. Engerer, J. H. Doty and T. S. Fisher, “Transient thermal analysis of flash-boiling cooling in the presence of high-heat-flux loads,” *International Journal of Heat and Mass Transfer*, vol. 123, pp. 678-692, 2018.

[4.8.1] D. Sterratt, B. Graham, A. Gillies, and D. Willshaw, “The synapse,” in *Principles of Computational Modelling in Neuroscience*, Cambridge, UK: Cambridge University Press, 2011, ch. 7, pp. 172–195.

[A.1.1] *Chemical Compatibility Database*, Cole-Parmer Instrument Company, Accessed on: May 20, 2021. [Online]. Available: https://www.coleparmer.com/chemical-resistance